

AD-750 742

THE INDUCTION ARC, A STATE-OF-THE-ART  
REVIEW

Hans U. Eckert

Aerospace Corporation

Prepared for:

Space and Missile Systems Organization

31 October 1972

DISTRIBUTED BY:

**NTIS**

**National Technical Information Service**  
**U. S. DEPARTMENT OF COMMERCE**  
5285 Port Royal Road, Springfield Va. 22151

AD 750742

# The Induction Arc A State-of-the-Art Review

Prepared by H. U. ECKERT  
Plasma Research Laboratory

72 OCT 31

---

Laboratory Operations  
THE AEROSPACE CORPORATION

---



Prepared for SPACE AND MISSILE SYSTEMS ORGANIZATION  
AIR FORCE SYSTEMS COMMAND  
LOS ANGELES AIR FORCE STATION  
Los Angeles, California

Reproduced by  
NATIONAL TECHNICAL  
INFORMATION SERVICE  
U.S. Department of Commerce  
Springfield VA 22151

APPROVED FOR PUBLIC RELEASE:  
DISTRIBUTION UNLIMITED

78

## LABORATORY OPERATIONS

The Laboratory Operations of The Aerospace Corporation is conducting experimental and theoretical investigations necessary for the evaluation and application of scientific advances to new military concepts and systems. Versatility and flexibility have been developed to a high degree by the laboratory personnel in dealing with the many problems encountered in the nation's rapidly developing space and missile systems. Expertise in the latest scientific developments is vital to the accomplishment of tasks related to these problems. The laboratories that contribute to this research are:

Aerodynamics and Propulsion Research Laboratory: Launch and reentry aerodynamics, heat transfer, reentry physics, propulsion, high-temperature chemistry and chemical kinetics, structural mechanics, flight dynamics, atmospheric pollution, and high-power gas lasers.

Electronics Research Laboratory: Generation, transmission, detection, and processing of electromagnetic radiation in the terrestrial and space environments, with emphasis on the millimeter-wave, infrared, and visible portions of the spectrum; design and fabrication of antennas, complex optical systems and photolithographic solid-state devices; test and development of practical superconducting detectors and laser devices and technology, including high-power lasers, atmospheric pollution, and biomedical problems.

Materials Sciences Laboratory: Development of new materials; metal matrix composites and new forms of carbon; test and evaluation of graphite and ceramics in reentry; spacecraft materials and components in radiation and high-vacuum environments; application of fracture mechanics to stress corrosion and fatigue-induced fractures in structural metals; effect of nature of material surfaces on lubrication, photosensitization, and catalytic reactions, and development of prosthesis devices.

Plasma Research Laboratory: Reentry physics and nuclear weapons effects; the interaction of antennas with reentry plasma sheaths; experimentation with thermonuclear plasmas; the generation and propagation of plasma waves in the magnetosphere; chemical reactions of vibrationally excited species in rocket plumes; and high-precision laser ranging.

Space Physics Laboratory: Astronomy; density and composition of the atmosphere at all altitudes; atmospheric reactions and atmospheric optics; pollution of the environment; the sun, earth's resources; meteorological measurements; radiation belts and cosmic rays; and the effects of nuclear explosions, magnetic storms, and solar radiation on the atmosphere.

THE AEROSPACE CORPORATION  
El Segundo, California

ACCESSION for	White Section <input checked="" type="checkbox"/>
NTIS	Buff Section <input type="checkbox"/>
DDC	<input type="checkbox"/>
UNANNOUNCED	
JUSTIFICATION	
BY	
DISTRIBUTION/AVAILABILITY	
file	AVAIL & FILE
A	

UNCLASSIFIED

Security Classification

DOCUMENT CONTROL DATA - R & D

(Security classification of title, body of abstract and indexing annotation must be entered when the overall report is classified)

1. ORIGINATING ACTIVITY (Corporate author)

The Aerospace Corporation  
El Segundo, California

2a. REPORT SECURITY CLASSIFICATION

Unclassified

2b. GROUP

3. REPORT TITLE

The Induction Arc, A State-of-the-Arc Review

4. DESCRIPTIVE NOTES (Type of report and inclusive dates)

5. AUTHOR(S) (First name, middle initial, last name)

Hans U. Eckert

6. REPORT DATE

72 OCT 31

7a. TOTAL NO. OF PAGES

80

7b. NO. OF REFS

119

8a. CONTRACT OR GRANT NO.

FO4701-72-C-0073

b. PROJECT NO.

c.

d.

9a. ORIGINATOR'S REPORT NUMBER(S)

TR-0073(3220-20)-2

9b. OTHER REPORT NO(S) (Any other numbers that may be assigned this report)

SAMSO-TR-72-227

10. DISTRIBUTION STATEMENT

Approved for public release; distribution unlimited

11. SUPPLEMENTARY NOTES

Details of illustrations in  
this document may be better  
studied on microfiche.

12. SPONSORING MILITARY ACTIVITY

Space and Missile Systems Organization  
Air Force Systems Command  
Los Angeles, California

13. ABSTRACT

The induction arc is, in principle, a high-frequency transformer in which the secondary is formed by a thermal plasma. Since its invention in 1961, this arc has been the subject of over 100 investigations with widely differing goals. Information contained in the literature up to 1972, covering history, experimental techniques, theory, and applications, has been collected and reviewed. Fair agreement between experimental and theoretical data indicates that heat balance and skin effect are the two basic processes governing the arc plasma. This agreement appears to be limited by non-equilibrium effects for which no provisions have been made in the theoretical models. The absence of contamination by electrode material makes the induction arc suitable for applications where a clean plasma is essential. The most important industrial application may be in plasma chemistry, provided such an arc can be operated more efficiently. A promising approach is low-frequency operation directly from the power line by means of a sufficiently large iron core.

1

14.

KEY WORDS

Applications  
Argon Plasma  
Electrodeless Discharge  
Induction Torch  
Nonequilibrium Effects

Distribution Statement (Continued)

Abstract (Continued)

Air Force Report No.  
SAMSO-TR-72-227

Aerospace Report No.  
TR-0073(3220-20)-2

THE INDUCTION ARC  
A STATE-OF-THE-ART REVIEW

Prepared by  
H. U. Eckert  
Plasma Research Laboratory

72 OCT 31

Laboratory Operations  
THE AEROSPACE CORPORATION

Prepared for  
SPACE AND MISSILE SYSTEMS ORGANIZATION  
AIR FORCE SYSTEMS COMMAND  
LOS ANGELES AIR FORCE STATION  
Los Angeles, California

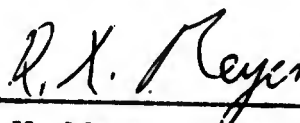
Approved for public release; distribution unlimited.

## FOREWORD

This report is published by The Aerospace Corporation, El Segundo, California, under Air Force Contract No. F04701-72-C-0073.

This report, which documents research carried out from February through June 1972, was submitted for review and approval on 30 August 1972 to Lt Col Elliott W. Porter, DYX.

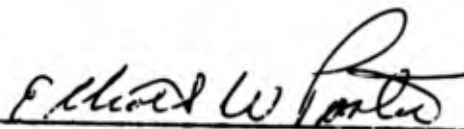
Approved



---

R. X. Meyer, Director  
Plasma Research Laboratory

Publication of this report does not constitute Air Force approval of the report's findings or conclusions. It is published only for the exchange and stimulation of ideas.



---

Elliott W. Porter, Lt Col, USAF  
Asst Director  
Development Directorate  
Deputy for Technology

## CONTENTS

FOREWORD . . . . .	ii
ABSTRACT . . . . .	iii
NOMENCLATURE . . . . .	ix
I. INTRODUCTION . . . . .	1
A. General . . . . .	1
B. History . . . . .	2
II. EXPERIMENTAL CONSIDERATIONS . . . . .	5
A. Starting an Induction Arc . . . . .	5
B. Earlier Experiments, Stability of the Discharge . . . . .	5
C. Diagnostics . . . . .	10
D. Arcs Above Atmospheric Pressure, Effects of a DC Magnetic Field . . . . .	16
III. THEORETICAL ANALYSIS . . . . .	23
A. Heat Balance . . . . .	23
B. Comparison with Experiment, Nonequilibrium Effects . . . . .	33
C. Two-Dimensional and Convection Effects, Magnetic Pumping . . . . .	36
IV. APPLICATIONS . . . . .	47
V. SUMMARY AND CONCLUSIONS . . . . .	59
REFERENCES . . . . .	61

## FIGURES

1.	Diagram of induction torch. . . . .	3
2.	Starting a large argon induction flame . . . . .	6
3.	Measured radial temperature distributions in several induction plasmas of different radii . . . . .	8
4.	Distribution of temperature and electric conductivity of induction plasma in a plane through the axis . . . . .	9
5.	Axial distribution of induced voltage without ( $\dot{\phi}_0$ ) and with plasma ( $\phi$ ) measured with loop shown at left. . . . .	12
6.	Enlarged tip section of water-cooled magnetic probe. . . . .	13
7.	Radial variation of rf magnetic field at midsection of inductor coil with and without plasma . . . . .	14
8.	Distribution of rf magnetic field on axis of discharge tube. . . .	15
9.	Polargram of rf magnetic field in plasma at inductor midsection . . . . .	17
10.	Polargram of electric field induced in plasma at inductor midsection . . . . .	18
11.	Distributions of $ E $ , $ j $ , and $\sigma$ over radius of plasma column at inductor midsection . . . . .	19
12.	Fraction of power lost by radiation in xenon arc vs pressure . .	20
13.	Effect of dc magnetic field on induction arc . . . . .	22
14.	Directions of electric field E, magnetic field H, and Poynting vector S in induction-heated cylinder . . . . .	24
15.	Variation of temperature integral $\left[ \int_0^T \sigma(T) \kappa(T) dT \right]^{1/2}$ with temperature for argon, nitrogen, and oxygen. . . . .	27
16.	Comparison between temperatures determined by spectroscopy and by magnetic probes with use of Fig. 15 . . . . .	28

Preceding page blank

17.	Comparison between spectroscopically determined temperatures, numerical calculations, and closed-form solutions by two-zone model . . . . .	30
18.	Results of numerical integration of Eq. (27) . . . . .	34
19.	Computed temperature fields in axial flow for three power levels. . . . .	38
20.	Temperature field calculated by quasi-one-dimensional approach from axial magnetic field distribution . . . . .	39
21.	Induction flame with radial gas supply . . . . .	41
22.	Flow pattern and velocities in induction flame . . . . .	44
23.	Reflection of $10\mu$ alumina particles from top of induction flame . . . . .	45
24.	Correlation of electric conductivity data of Fig. 11 with equilibrium temperatures and comparison with results of other investigators . . . . .	48
25.	Schematic diagram of apparatus for crystal growth. . . . .	51
26.	Electrodeless lamp in spherical quartz enclosure. . . . .	52
27.	Starting phase of low frequency electrodeless arc in argon. . . . .	54
28.	Inductive electrodeless arc in argon . . . . .	55
29.	Minimum values of magnetic core radius R and tube radius r for maintaining electrodeless arc in argon at $p = 1$ atm for several magnetic flux densities . . . . .	56

## NOMENCLATURE

A	integration constant Eqs. (17) and (39)
B	integration constant Eq. (39)
b	constant defined by Eq. (37)
c	constant defined by Eq. (15)
$c_p$	specific heat at constant pressure
D	inner diameter of discharge tube
E	rms value of induced electric field
f	driving frequency
H	rms value of driving magnetic field
I	electric current; also, ionization temperature
J	Bessel function of the first kind
j	current density
l	length of discharge column
n	electron density
P	power
p	pressure
Q	radiation source strength
q	exponent defined by Eq. (16)
R	plasma radius
r	radial coordinate
S	electromagnetic energy flux
s	heat conduction potential defined by Eq. (13)
T	temperature
u	velocity
V	induced voltage
Y	Bessel function of second kind
Z	combined Bessel functions defined by Eq. (39)
z	axial coordinate

### Greek letters

$\alpha$	electron-ion recombination coefficient defined by Eq. (42)
$\delta$	skin depth $\equiv \left(\frac{2}{\sigma\mu\omega}\right)^{\frac{1}{2}}$
$\zeta$	nondimensional radial coordinate defined by Eq. (26)
$\theta$	nondimensional temperature defined by Eq. (25)
$\kappa$	thermal conductivity
$\lambda$	eigenvalue in heat balance equation defined by Eq. (18)
$\mu$	magnetic permeability
$\mu_0$	magnetic permeability of vacuum
$\rho$	density
$\sigma$	electric conductivity
$\phi$	magnetic flux
$\omega$	angular frequency $\equiv 2\pi f$

### Subscripts

m	maximum value
o	refers to conditions at $r = 0$ unless otherwise specified in text; also, zero order Bessel function
r	refers to radial direction
R	refers to conditions at $r = R$
z	refers to axial direction
$\theta$	refers to azimuthal direction
1	refers to primary circuit
2	refers to secondary circuit

## I. INTRODUCTION

### A. GENERAL

The induction arc, also known as electrodeless arc or thermal induction plasma, represents a special type of high-pressure discharge in which the sustaining power is supplied by induction from a time-varying magnetic field. It may be considered as a transformer where the secondary winding consists of a single turn formed by the arc plasma. The primary consists of a cylindrical or (less frequently) a flat multiturn coil that generally also represents the inductance for the plate tank circuit of a vacuum tube oscillator. The arc is contained in a quartz or sometimes a slotted metal tube. Frequencies range from about 50 MHz for the smallest arcs (tube diam  $D \sim 1$  cm) to about 0.2 MHz for large arcs ( $D \sim 20$  cm). Because the frequency is high compared with the decay rate of the discharge, the plasma has steady or quasi-steady character.

As a clean plasma source, the induction arc has become of interest to physicists, chemists, and engineers, and the literature in the past ten years has swelled to several hundred articles. This information is scattered in many reports and journals of various disciplines and national origin. As a result, it is becoming more and more difficult to survey the state of the art. It was, therefore, considered a timely undertaking to collect and digest the literature and to make it available in a review paper to allow scientific and technical groups, which often seem to have been unaware of each other, to learn about each other's work, share the accomplishments, and avoid duplication. Because of space and time limitations, not all of the reference items could be cited in the text, and the reader in search of special information is advised to carefully examine the Reference Section. Conversely, some heretofore unpublished material is presented that serves to round out the still sketchy picture of the induction arc.

As the overwhelming majority of all experimental and theoretical work has been done with argon at atmospheric pressure, all of the results that

involve gas properties refer to these conditions unless stated otherwise.

Data, including arcs in air,  $N_2$ , and  $O_2$ , are contained in Refs. [3, 11, 34, 39, 40, 43, 53, 61, 67, 83, 84, 100, 101, 102]; for data on xenon arcs, see Refs. [45, 46, 75, 77, 94, 95, 96]; for krypton, [75, 77]; for neon, [75, 77].

## B. HISTORY

In contrast to the history of dc discharges where arcs and glow discharges had an independent development, the induction arc is an outgrowth of the low-pressure electrodeless ring discharge. The latter was discovered in 1884 by Hittorf [51] in experiments on the conduction of electricity through rarefied gases. Trains of damped, high-frequency oscillations were generated by periodically charging Leyden jars with a spark inductor and discharging the jars through a coil that surrounded a Geissler tube. Thomson [108] experimented for many years with an arrangement of this kind; in 1927, he published his results and a theory of the electrodeless discharge in which the plasma conductivity across the column is considered constant. This enabled him to express the magnetic and electric field distributions by Bessel functions. Because of its convenience, this model is still used frequently in approximate analyses of induction arcs. Babat [3], operating with a powerful vacuum tube oscillator, discovered in 1942 that a ring discharge, once established, can be maintained while the pressure is raised up to atmospheric level and thereby converted into an arc discharge. Babat is thus the inventor of the induction arc. However, major interest developed only after Reed [85] had shown in 1961 that, with an open tube and streaming gas, one can produce an "induction torch" where the plasma is directly observable and can be used as a heat source as shown in Fig. 1. One application demonstrated by Reed is the growing of crystals of refractory materials [86]. He also measured heat transfer rates from argon induction flames to a probe and found them comparable to that from oxy-hydrogen flames of the same power level [87]. (For a similar investigation with an air induction torch, see Ref. [61].)

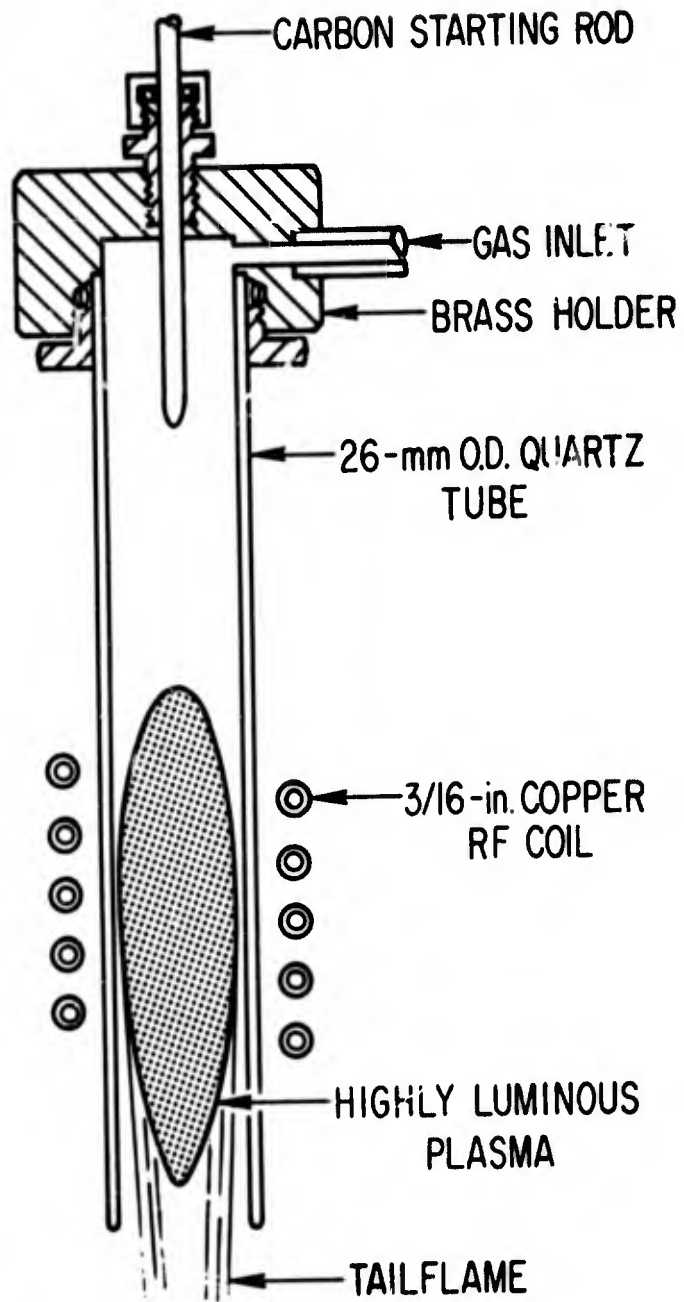


Fig. 1. Diagram of induction torch after Reed [85].

## II. EXPERIMENTAL CONSIDERATIONS

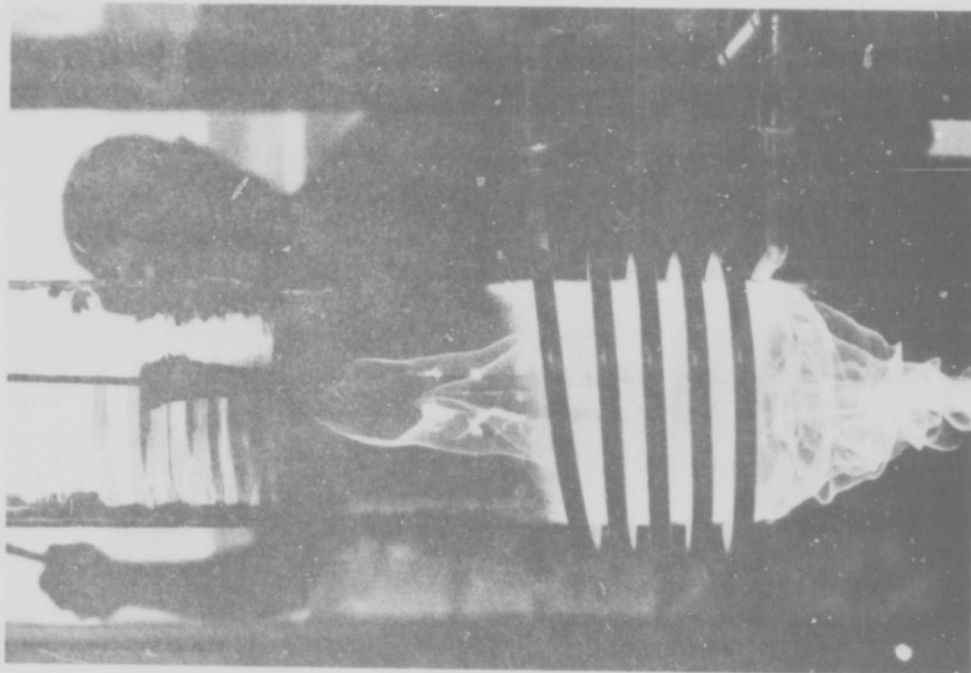
### A. STARTING AN INDUCTION ARC

Transfer of energy from the alternating magnetic field to the gas requires the existence of a closed conducting loop so that a current is produced by the induced voltage. If the voltage at the discharge tube periphery exceeds 100 V, the gas will usually break down at pressures around 1 Torr and the pressure can subsequently be raised to establish a thermal plasma [3, 39]. In the method employed by Reed [85] to start a small argon torch at atmospheric pressure (Fig. 1), a carbon rod is inserted into the inductor field. In this case, heating of the carbon by the induced currents lowers the density of the adjacent gas and promotes breakdown, especially if the surface is hot enough to allow appreciable electron emission.

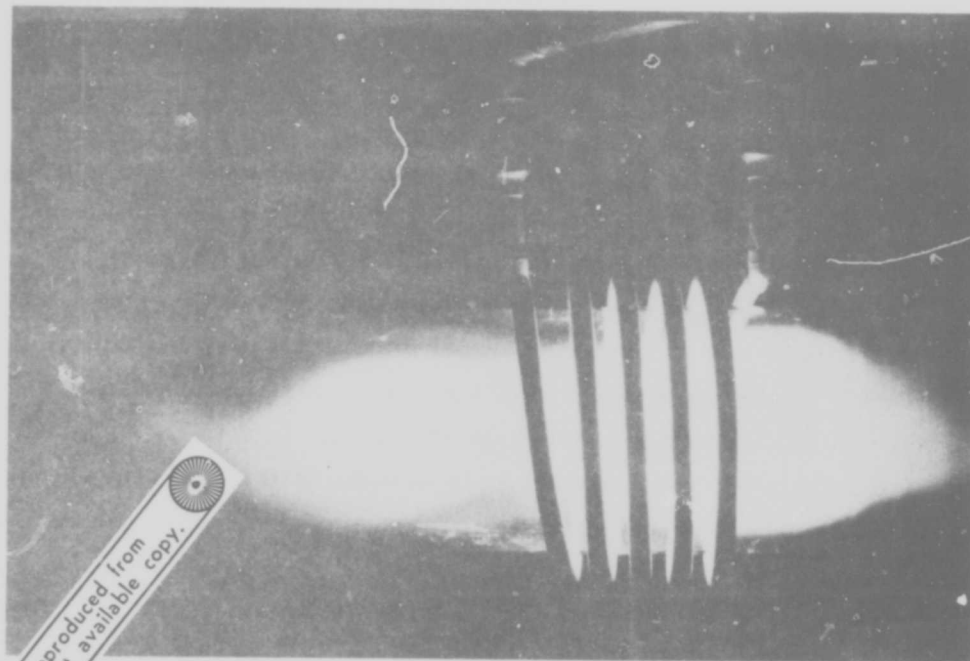
For large tube diameters, it is more convenient to bring a wire of tungsten or other refractory metal into the tube near the end of the inductor coil that carries a high rf potential against ground. This permits a capacitive current to flow between coil and wire through the tube dielectric. If the wire is now moved into the tube inferior, a filamentary arc is drawn which, depending on the kind of gas and coil potential, may become as long as 1 m. Breakdown is facilitated if the gas is introduced in a swirl motion, as this gives a better chance for formation of a closed loop. A time exposure of rotating filaments in a 150-mm wide tube is shown in Fig. 2a. In Fig. 2b, the fully developed plasma flame is shown. The latter two starting methods are preferably used with argon as supply gas. After the discharge is established, one can gradually change over to other gases such as oxygen or nitrogen. The starting methods and pressures have been discussed by Arsen'ev and Kustov [2] .

### B. EARLIER EXPERIMENTS, STABILITY OF THE DISCHARGE

Soon after Reed had published his results on the induction torch, other workers in the U.S., Great Britain, France, and primarily in the Soviet Union began to test similar devices, using mainly argon. A number of spectroscopic



(a) Rotating filaments drawn by carbon rod



(b) Established plasma flame

Fig. 2. Starting a large argon induction flame.

Reproduced from  
best available copy.

investigations were carried out, and temperature distributions were derived on the assumption of thermal equilibrium throughout the plasma. It was soon recognized [27, 42, 53, 78] that the intensity maximum of line radiation observed near the plasma boundary was not of the Larenz type as Reed [85] had assumed but was caused by skin heating and radiation cooling. Maximum temperatures ranged between 8000 and 11000 K, with the higher temperatures generally existing in the smaller tubes.

Radial profiles, obtained by several authors, at the maximum cross section of the discharge are presented in Fig. 3. A plot of an entire temperature field measured by Goldfarb and Dresvin [42] is shown in Fig. 4. The good agreement obtained from line and continuum radiation, as well as from Stark broadening of impurity lines (mostly the  $H_{\beta}$  line), was taken as a confirmation of the existence of thermal equilibrium. Discrepancies arose, however, when some workers compared spectroscopically derived temperatures with results from calorimetry [21, 9] or probes [44], which were lower by up to 30%. This would indicate some lack of equilibrium in the plasma and will be discussed in Sec. III.

Dymshits and Koretskii [27] reported that, in their experiments, the ratio of plasma radius to skin depth  $R/\delta$  changed between 1.65 and 1.75 only; although frequency, pressure, tube radius, and flow rate were varied over considerable ranges. The interpretation of this result has caused some controversy. From the theory of induction heating of metals, it is well known that  $R/\delta = 1.75$  represents the optimum efficiency in power transmission to the load ( $\approx 37\%$ ). At larger values of  $\delta$ , corresponding to lower frequencies  $f$ , the magnetic field can penetrate deeper into the medium, but the induced electric fields, being proportional to  $f$ , are also lower. At higher values of  $f$ , the induced fields and currents are correspondingly higher and shield out the magnetic field ( $\delta$  small).

The best compromise exists at  $R/\delta = 1.75$ . In a solid conductor, this ratio is practically independent of the applied magnetic field and power input. However, in a plasma,  $\delta$  and, to a lesser extent,  $R$  vary with power input  $P$  so that  $R/\delta$  depends on this parameter as well as on  $f$ . One can now argue that,

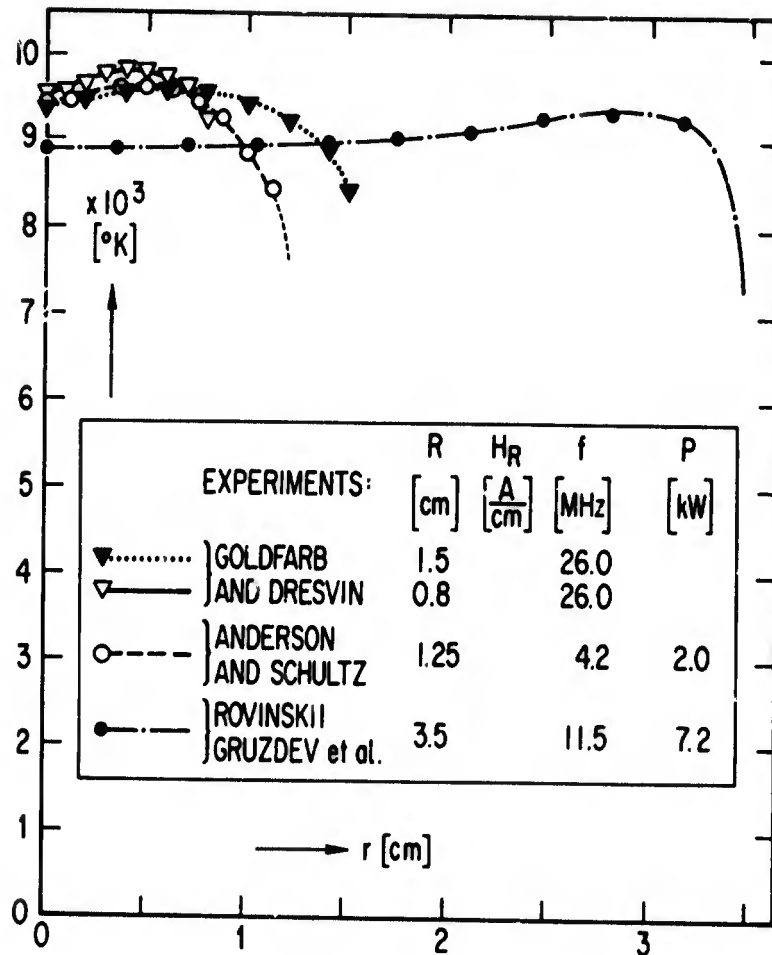


Fig. 3. Measured radial temperature distributions in several induction plasmas of different radii [42, 96, 97].

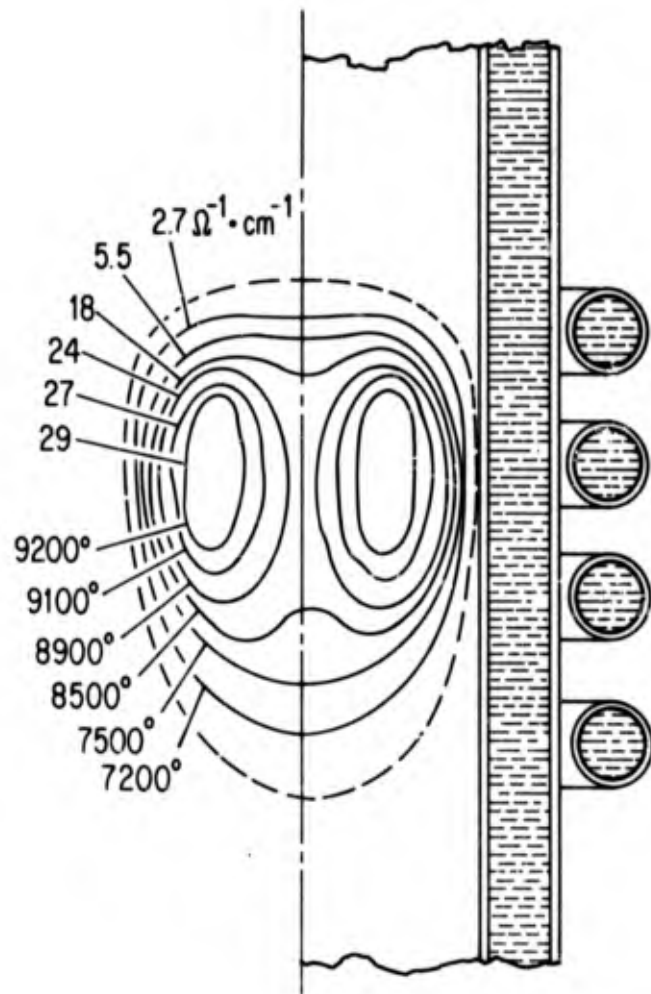


Fig. 4. Distribution of temperature and electric conductivity of induction plasma in a plane through the axis [42].

for a plasma, the rising branch of the efficiency curve, where  $R/\delta < 1.75$ , is unstable. If we imagine a steady discharge to exist at a point of this branch and allow, for instance, a slight increase in  $P$  to occur by an increase of the applied magnetic field  $H_R$ , the conductivity  $\sigma$  would increase,  $\delta$  would decrease, and the discharge would move to a point of higher  $R/\delta$  (i. e., of higher efficiency) on the curve. This means increased power input for the same  $H_R$  to which the discharge must respond by a further increase in  $\sigma$ . This results in a still larger  $R/\delta$  and improved efficiency and so on, until the maximum is obtained. Conversely, a slight reduction in power input would cause the discharge to move in the opposite direction and extinguish it.

A discharge with  $R/\delta > 1.75$  will be stable because here an increase in the applied field, causing  $\sigma$  and  $R/\delta$  to rise, will lead to a decrease in power transfer efficiency that will counteract the field increase. A decrease in the field can be carried to the point where  $R/\delta \sim 1.75$ ; a further decrease will extinguish the discharge. The results of Dymshits and Koretskii [27] can therefore be understood if it is assumed that their discharges have always been operated at minimum power. In addition to this skin effect phenomenon, gas properties, geometry, and generator characteristics may affect the stability. For a recent contribution to solving this problem, see [118]. If one searches the literature, many cases can be found where  $R/\delta$  has been appreciably larger than 1.75 but none where it has been appreciably less. This indicates that skin effect is the dominant phenomenon for discharge stability.

### C. DIAGNOSTICS

Most diagnostic work on induction arcs consisted of determining electron temperatures by means of spectroscopy. As these techniques do not differ from those used on regular arcs, they need not be discussed here. However, it may be mentioned that, because of the generally lower temperatures, not only emission but also absorption can be used for their determination. Johnson [58] used a flashtube as a background light source to measure absorption coefficients of the Al 7635 Å and 7514 Å lines.

Atom temperatures were determined from Doppler-broadened argon lines by Kleinmann and Cajko [60]. Henderson [49] deduced gas temperatures from the shock standoff distance of nylon spheres that were fired through the plasma at supersonic velocities.

Measurement of the maintenance voltage of an induction arc is more difficult than that of a dc arc. This has been done [32] with a water-cooled wire loop embedded in a quartz capillary as shown in Fig. 5. The figure also shows the axial distributions of the induced voltages without and with the plasma, designated by  $\Phi_0$  and  $\Phi$ , respectively, because the voltage is identical in magnitude with the time rate of change of the magnetic flux through the loop.

The magnetic probe is a diagnostic tool that is especially suited for the induction arc and that has yielded valuable information about its structure. It consists of a multiturn miniature coil embedded in a capillary that is inserted into the arc plasma. At a constant operating frequency, the probe delivers a signal proportional to the local value of the magnetic field. In order to obtain good spatial resolution and to keep the perturbation of the plasma small, it is important that the diameter of the probe stem is small compared with that of the plasma column. A water-cooled version of a probe designed for continuous operation is presented in Fig. 6, and its design and performance are described in detail in Ref. [35]. In other work [109], a spring-operated injection and retraction mechanism has been developed for use with uncooled probes. In Fig. 7 is shown the radial distributions of  $|H|$  without and with plasma obtained with the probe of Fig. 6. The plasma flame was similar to that shown in Fig. 2b. The slight dip of  $|H|$  in the unloaded case and the excessive values near the walls in the loaded case are both due to the finite length of the inductor coil [35]. In Fig. 8 is shown the axial distributions of  $H$  in argon and air plasmas, as well as in the unloaded coil [109]. The power input is the same for both plasmas, but the air plasma, which requires a higher induced electric field for maintenance, has the higher magnetic field at the axis. This means that the current in the air plasma is lower. With higher maintenance field and lower current, the impedance of the air plasma must be considerably higher than that of the argon plasma.

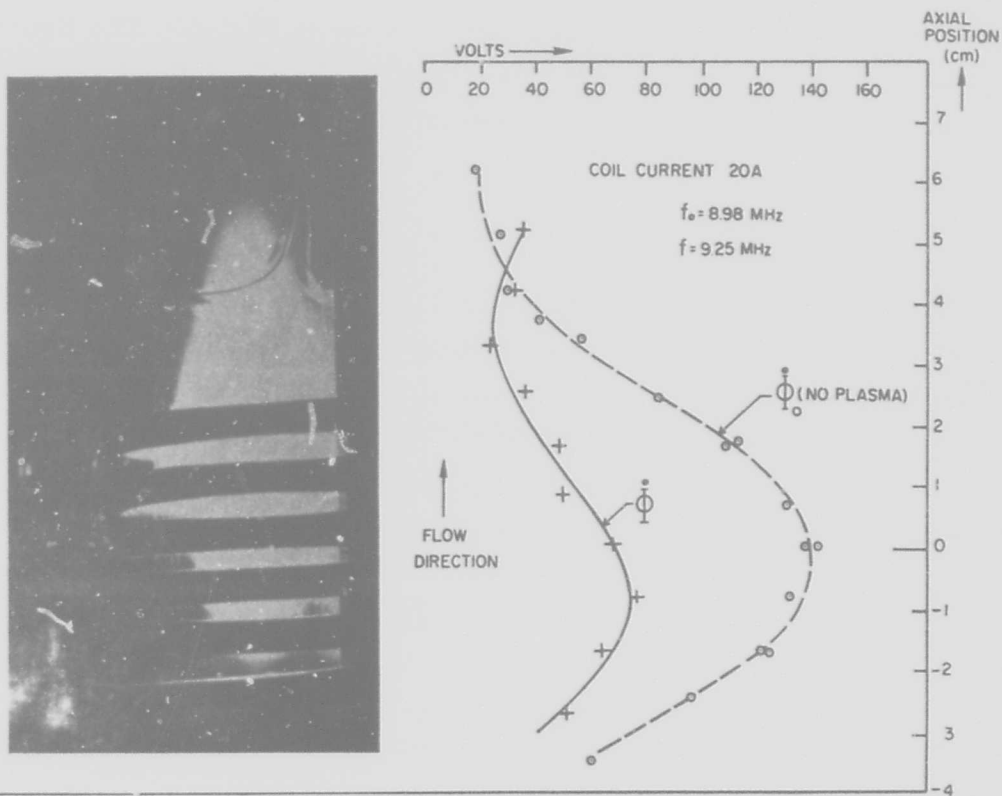


Fig. 5. Axial distribution of induced voltage without ( $\phi$ ) and with plasma ( $\phi$ ) measured with loop shown at left [32] ( $f = 8.3$  MHz,  $I_1 = 21$  A,  $P \sim 2.5$  kW).

Reproduced from  
best available copy.

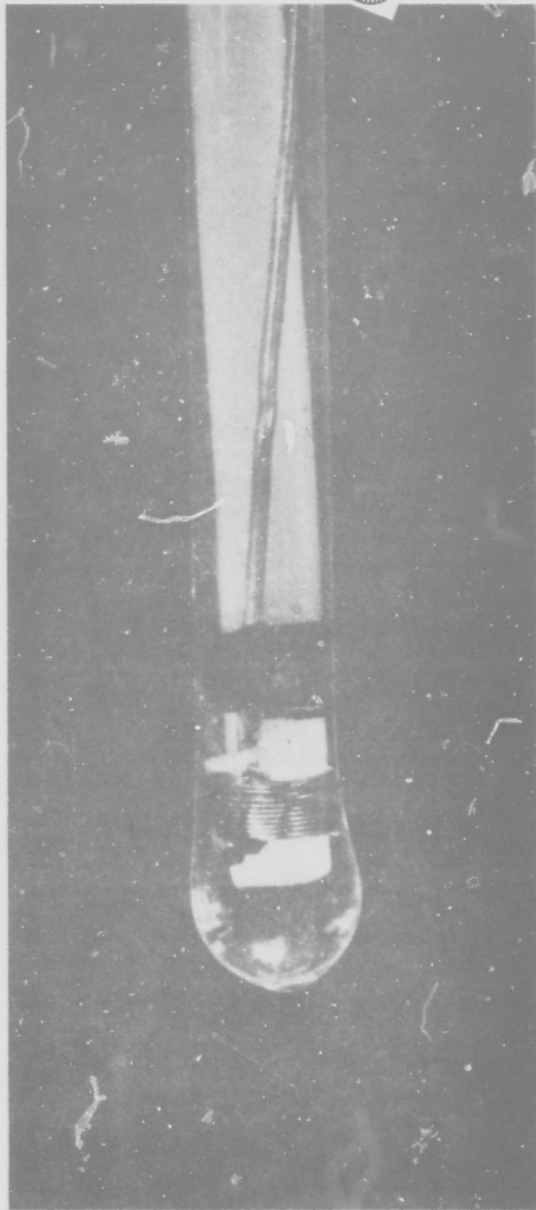


Fig. 6. Enlarged tip section of water-cooled magnetic probe.  
(Shaft diam. 0.4 cm) (For details, see [35] ).

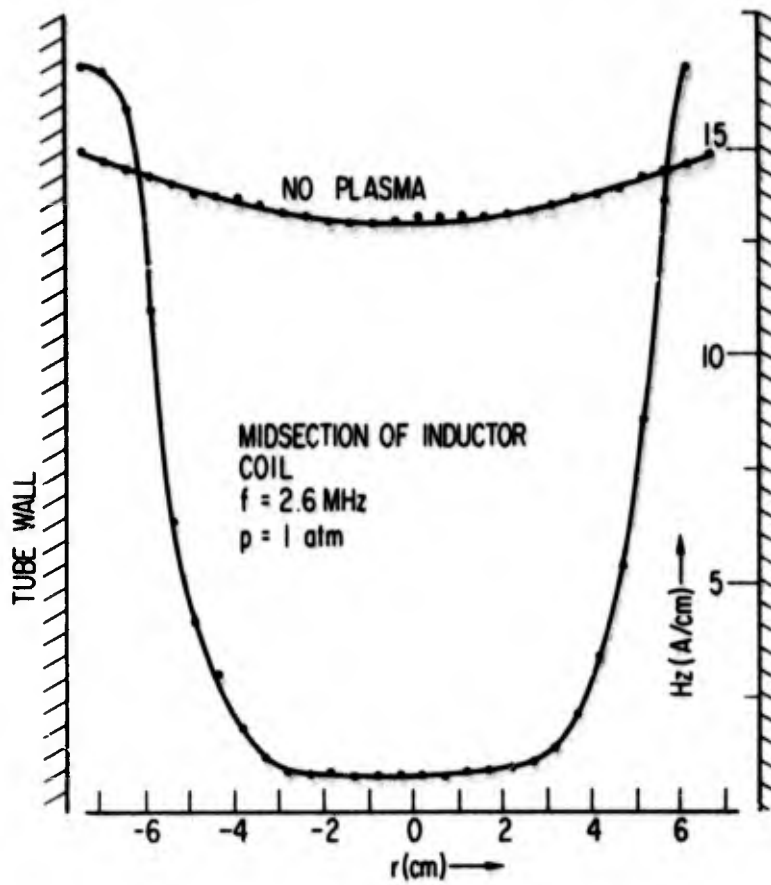


Fig. 7. Radial variation of rf magnetic field at midsection of inductor coil with and without plasma [35] ( $f = 2.6 \text{ MHz}$ ,  $I_1 = 68 \text{ A}$ ).

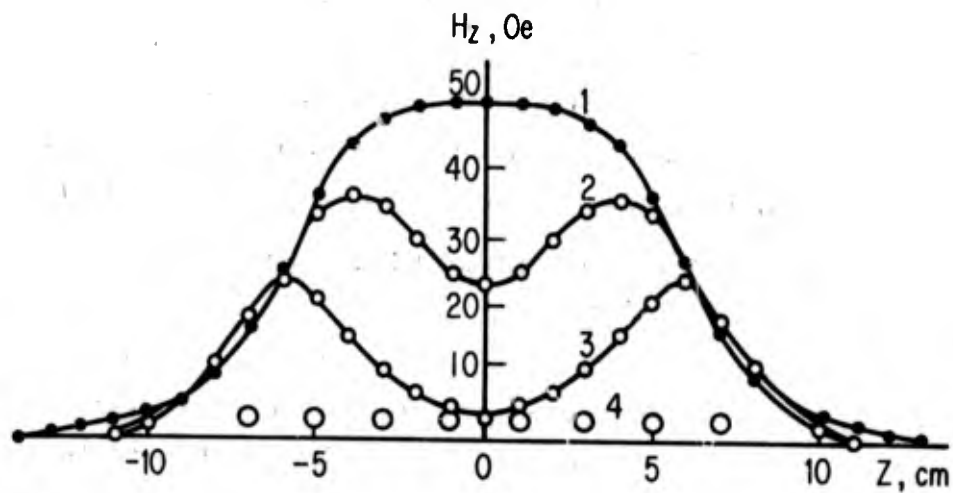


Fig. 8. Distribution of rf magnetic field on axis of discharge tube [109]. (1) Without plasma, (2) in air plasma, (3) in argon plasma, and (4) inductor ( $f = 9$  MHz,  $I_1 = 85$  A,  $R = 1.3$  cm,  $H_R = 45$  A/cm,  $P = 127$  kW).

As  $H$  is complex, one can obtain complete information about the electric conditions in the discharge only if the phase angle is also measured. A dual magnetic probe system to accomplish this is described in Ref. [36]. In addition to the movable probe measuring  $|H|$ , a fixed identical probe is placed at the boundary of the plasma column to measure  $H_R$ . The phase angle between the two signals is calculated from  $H_R$ ,  $|H|$ , and the vector sum or difference of the two signals. The distribution of real and imaginary components of  $H$  obtained in this manner is shown in Fig. 9 for conditions similar to those in Fig. 7. By integration of  $H$  over  $r$ , one obtains, according to Eq. (2) in the following section, the distribution of the induced electric field  $E$ , which is shown in Fig. 10. By differentiation of  $H$ , one obtains, according to Eq. (3), current density  $j$ . By the ratio  $j/E$ , one then has determined the electric conductivity  $\sigma$ . The distributions of  $|E|$ ,  $|j|$ , and  $\sigma$  are plotted in Fig. 11.

#### D. ARCS ABOVE ATMOSPHERIC PRESSURE, EFFECTS OF A DC MAGNETIC FIELD

Mitin and Pryadkin [74, 75] and Pryadkin, Mitin, and Klimov [81] have demonstrated that induction arcs can be maintained at pressures many times higher than atmospheric and that the limit ( $\sim 40$  atm) is apparently set only by the strength of the envelope. With increasing pressure, the energy balance shifts toward higher radiation losses that eventually dominate over the losses by conduction. In a discharge of unusually high power ( $P > 100$  kW) and power density ( $\sim 10$  kW/cm<sup>3</sup>), Roman and Klein [89] observed that, at  $p = 11$  atm, nearly 75% of the input power was radiated through the silicon tube. Data obtained for xenon in a less powerful discharge in experiments by Gruzdev, Rovinskii, and Shirokova [95, 46] for  $p$  between 0.1 and 10 atm are shown in Fig. 12. The ratio of radiated to total discharge power can be represented for this range by the empirical formula

$$P_{\text{rad}} \approx (0.38 + 0.25 \log p) P \quad (1)$$

Mitin and Pryadkin [76, 77] also observed unexpected effects of a permanent magnet on high-pressure discharge ( $p \sim 1$  to 3 atm). As long as the plasmoid had a spherical or ellipsoidal shape, it displayed slightly paramagnetic behavior;

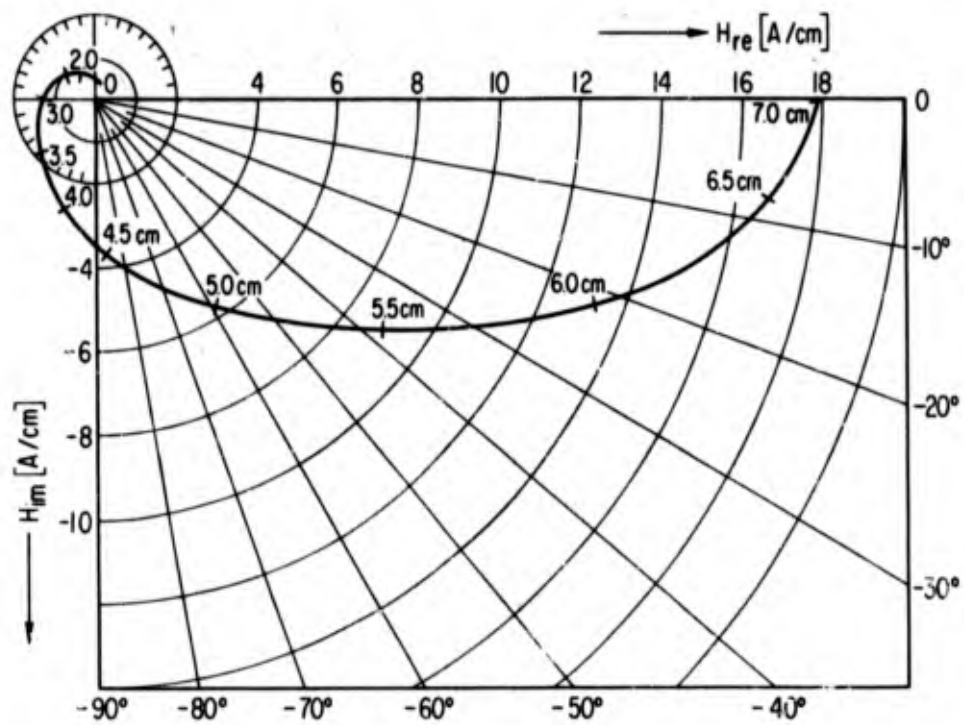


Fig. 9. Polargram of rf magnetic field in plasma at inductor midsection [36].

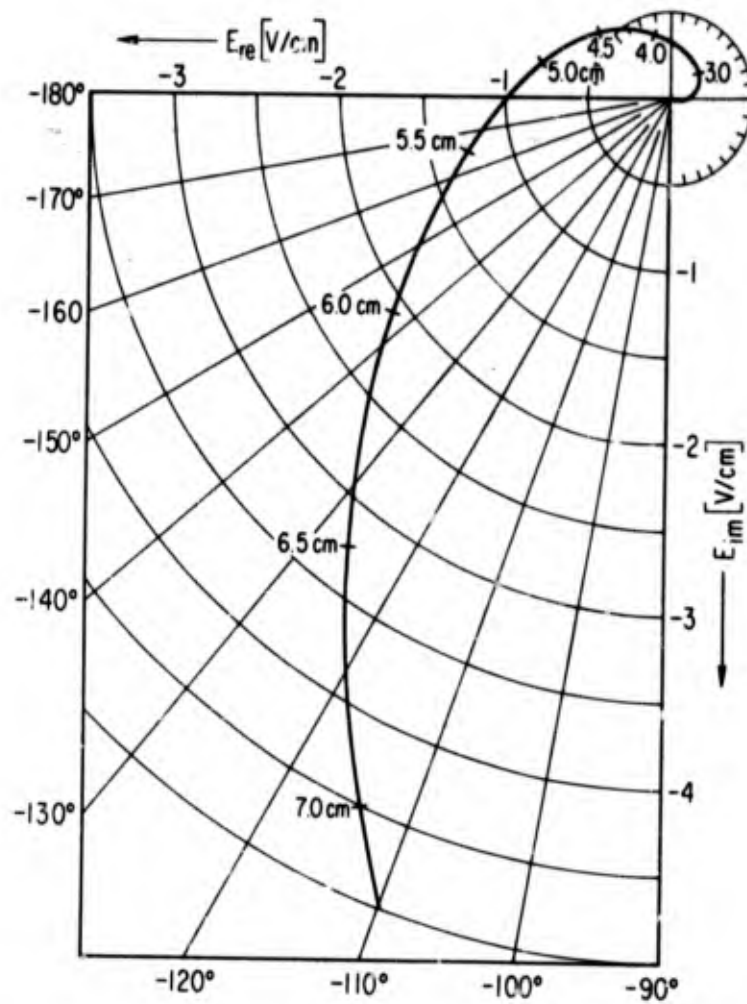


Fig. 10. Polargram of electric field induced in plasma at inductor midsection [36].

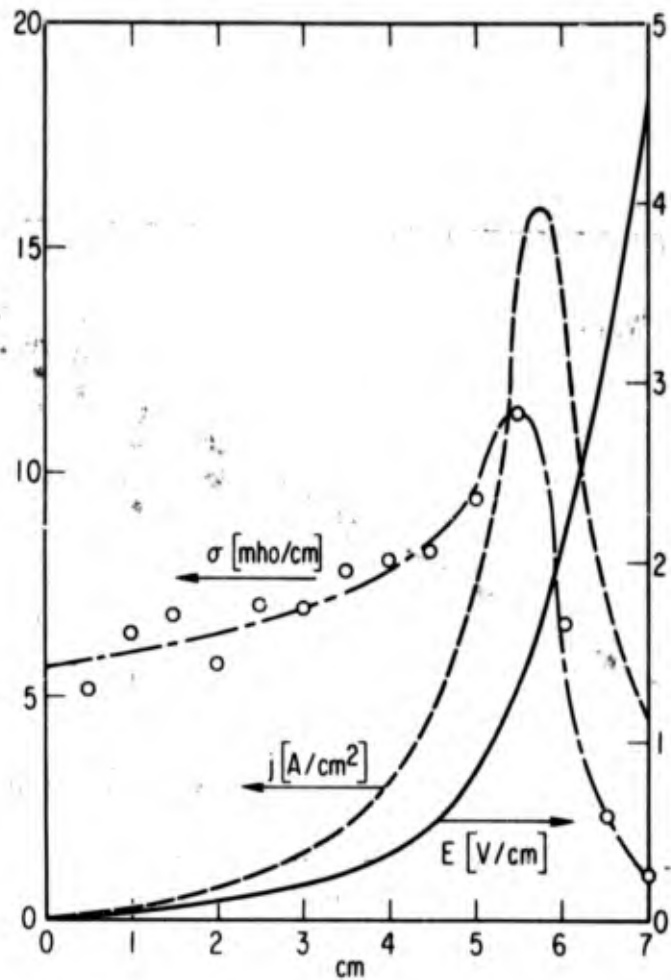


Fig. 11. Distributions of  $|E|$ ,  $|j|$ , and  $\sigma$  over radius of plasma column at inductor midsection [36].

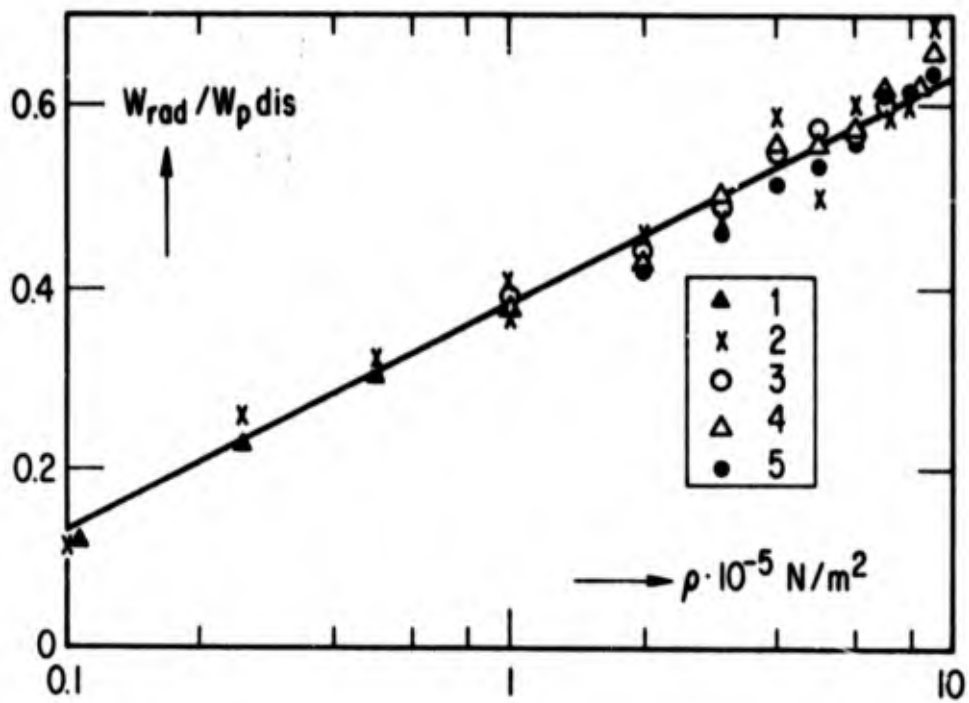


Fig. 12. Fraction of power lost by radiation in xenon arc vs pressure [95, 46].

that is, it was attracted by a magnet that, near the plasma, had a field strength of 200 to 300 A/cm and a gradient around  $100 \text{ A/cm}^2$ . In a stronger magnetic field, however, the plasmoid changed into a toroidal shape and then displayed diamagnetic behavior. The strength of these magnetic forces was estimated to be of the order of the thermal buoyancy of the plasmoid. From an estimate of the magnetic moment necessary to generate such forces at the existing field gradient and from the total rf current in the plasma, the authors conclude that a rectifying effect of the order of 1%, the direction of which depends on the shape of the plasmoid, can explain the observed behavior. Such an effect could be caused by the slight changes in plasmoid diameter in a dc magnetic field that favor one current half-period over the other. With further increases of the dc magnetic field, the toroid plane first assumes an inclination against that of the inductor turns, then starts to precess with increasing frequency, and finally becomes unstable and develops kinks, as shown in Fig. 13. This behavior is apparently caused by the tendency of the diamagnetic plasmoid to turn from an antiparallel to a parallel position.

Reproduced from  
best available copy.

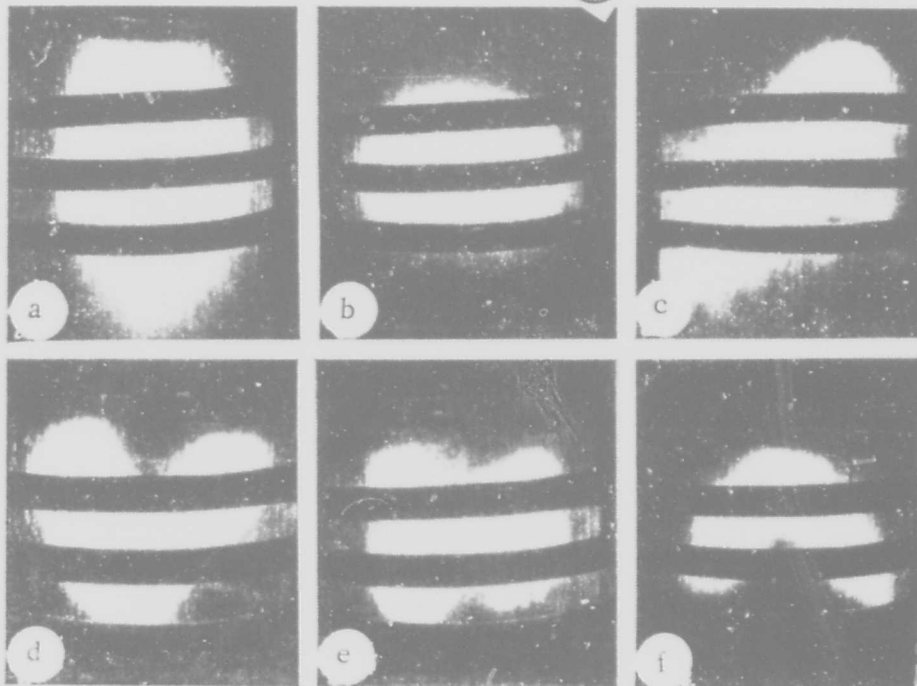


Fig. 13. Effect of dc magnetic field on induction arc.  
(a) Without magnetic field, (b) in weak field,  
(c-f) clot rotating in magnetic field [77].

### III. THEORETICAL ANALYSIS

#### A. HEAT BALANCE

The success with models for the dc arc based on the Elenbaas-Heller equation provided encouragement for similar analyses of the induction arc. Here the situation is more complicated as Maxwell's equations and Ohm's law must be satisfied. At a pressure of 1 atm, the electron collision frequency is by orders of magnitude higher than the driving frequency and the current is in phase with the electric field. As in the common arc, the heat generated by current dissipation is balanced in the steady state by heat losses due to conduction, convection, and radiation. In all the analyses for the induction arc known today, local thermal equilibrium has been assumed. The limitations of this assumption become apparent when results are compared with recent experimental data given in Sec. IIB.

In the common induction torches and flames with diameters of a few centimeters, operating near atmospheric pressure at gas velocities of the order of 1 m/sec, conduction to the wall is usually the principal loss process. In the beginning, therefore, we will disregard radiation and convection effects and consider only the balance between fluxes of electromagnetic power and heat conduction. This simplifies the situation and contributes to the understanding of the principle of an induction arc. We consider a section of an infinite plasma cylinder (Fig. 14) permeated axially by a magnetic field  $H = H_z$  that alternates at angular frequency  $\omega$  and, thereby, induces electric fields in aximuthal direction  $E \equiv E_\theta$  within the volume.  $H$  and  $E$  are related by Maxwell's equations, which, in the absence of displacement currents, have the following form:

$$\frac{1}{r} \frac{d}{dr} rE = -i\omega\mu H \quad (2)$$

and

$$\frac{dH}{dr} = -\sigma E = -j \quad (3)$$

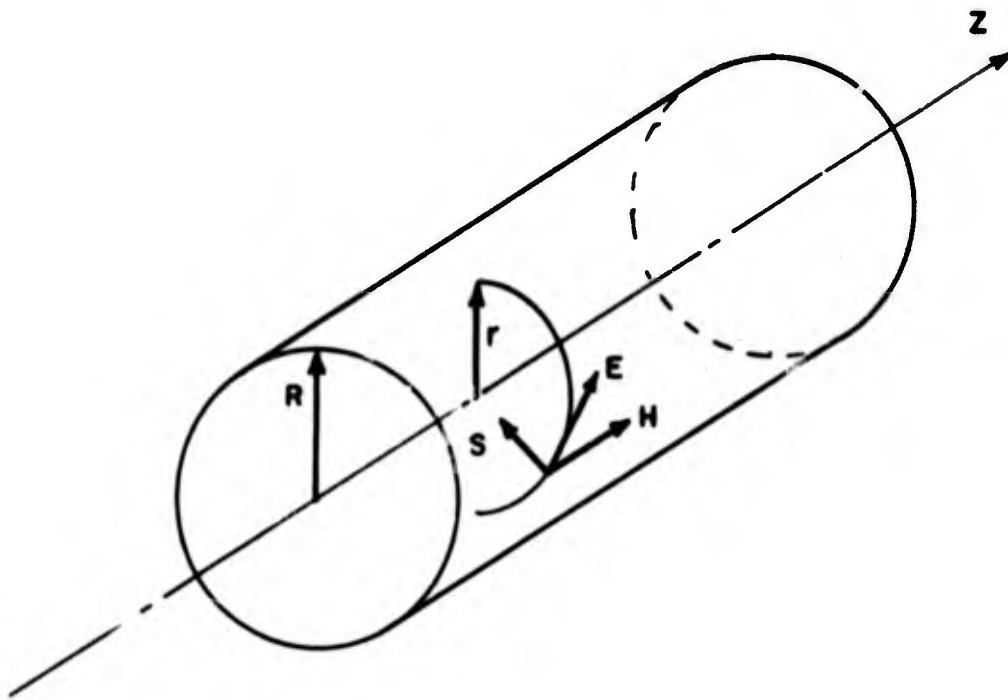


Fig. 14. Directions of electric field  $E$ , magnetic field  $H$ , and Poynting vector  $S$  in induction-heated cylinder.

Because E and H are complex, Eqs. (2) and (3) actually represent four equations in  $E_{re}$ ,  $E_{im}$ ,  $H_{re}$ ,  $H_{im}$ . The boundary conditions are

$$\frac{dH}{dr} = 0 \text{ at } r = 0; \quad H = H_{re} = H_R \text{ at } r = R \quad (4)(5)$$

Let us consider E and H as representing rms values. The Poynting vector  $S \equiv EH$  then represents the dissipative component of the electromagnetic energy flux density as only this component is nonvanishing when the average is taken. S is directed radially inward, as shown in Fig. 14. The divergence of this energy flux must, at any radial position, balance that of the heat flux  $-\kappa \frac{dT}{dr}$ , which is directed outward. Therefore,

$$\frac{1}{r} \frac{d}{dr} \left( rEH - r\kappa \frac{dT}{dr} \right) = 0 \quad (6)$$

As Raizer [84] has pointed out, it follows from integration of Eq. (6) and the fact that both fluxes vanish at  $r = 0$  that also

$$EH - \kappa \frac{dT}{dr} = 0 \quad (7)$$

that is, the fluxes of electromagnetic energy and heat balance each other at any point. We now combine Eqs. (5) and (3) to eliminate E and obtain

$$\frac{dT}{dr} + \frac{H}{\sigma} \frac{dH}{dr} = 0 \quad (8)$$

When Eq. (8) is rearranged and integrated from the outer boundary  $r = R$ , where  $T = T_R$  and  $H = H_R$  toward the interior, one obtains

$$\int_{T_R}^T \sigma(T) \kappa(T) dT = \frac{HR^2}{2} \left[ 1 - \left( \frac{H}{H_R} \right)^2 \right] \quad (9)$$

Thus, by evaluation of the integral in Eq. (9) and determination of the magnetic field distribution in the plasma, one can obtain the temperature distribution for a nonradiating column. This important result was first obtained by Gruzdev, Rovinskii, and Sobolev [47, 92]. Values of the square root of the integral in

Eq. (9) are plotted in Fig. 15 for argon, nitrogen, and oxygen at  $p = 1$  atm taken from Ref. [92]. In Fig. 16 is shown a comparison between spectroscopically determined temperatures [63] and temperatures obtained with Eq. (9) and Fig. 15 from probe measurements of the  $H(r)$  distribution in Fig. 7 [35]. In view of the fact that the magnetic method cannot account for radiation losses, the agreement must be considered satisfactory.

Determination of the field and temperature distributions entirely through calculation requires the solving of the complete Elenbaas-Heller equation, which, with the radiation term  $Q$  included, has the form

$$\frac{1}{r} \frac{d}{dr} r \frac{dT}{dr} + \sigma E^2 - Q = 0 \quad (10)$$

and the boundary conditions

$$\frac{dT}{dr} = 0 \text{ at } r = 0 \text{ and } T = T_R \text{ at } r = R \quad (11)(12)$$

Together with Eqs. (2) and (3), Eq. (10) forms a sixth order system. Much effort has been spent on its solution, using mainly numerical means. Soshnikov and Trekhov [100 through 102] and Hollister [53, 54] treated it as an initial value problem starting the integration at  $r = 0$  and terminating whenever  $T = 0$  or another reasonable value for  $T_R$  had been reached. The values of  $R$  and  $H_R$  thus follow from the solution. It is apparent, however, that a considerable number of trial runs may be required before the solution for specific values of  $R$  and  $H_R$  is obtained. In both these treatments, cases of air plasmas at ambient pressure were calculated. In addition to temperature profiles, Soshnikov and Trekhov also present magnitude and phase distributions of the magnetic and electric fields and of the current density. An attempt [102] to duplicate a temperature profile measured in a short argon plasma [42] was not successful. Better agreement was obtained more recently for an argon plasma with large length/diameter ratio [103]. Further comparison of results from this calculation method and experimental data from air and argon plasmas is presented in tabular form in a paper by Trekhov, Fomenko, and Koshev [109]. Agreement, in general, is satisfactory.

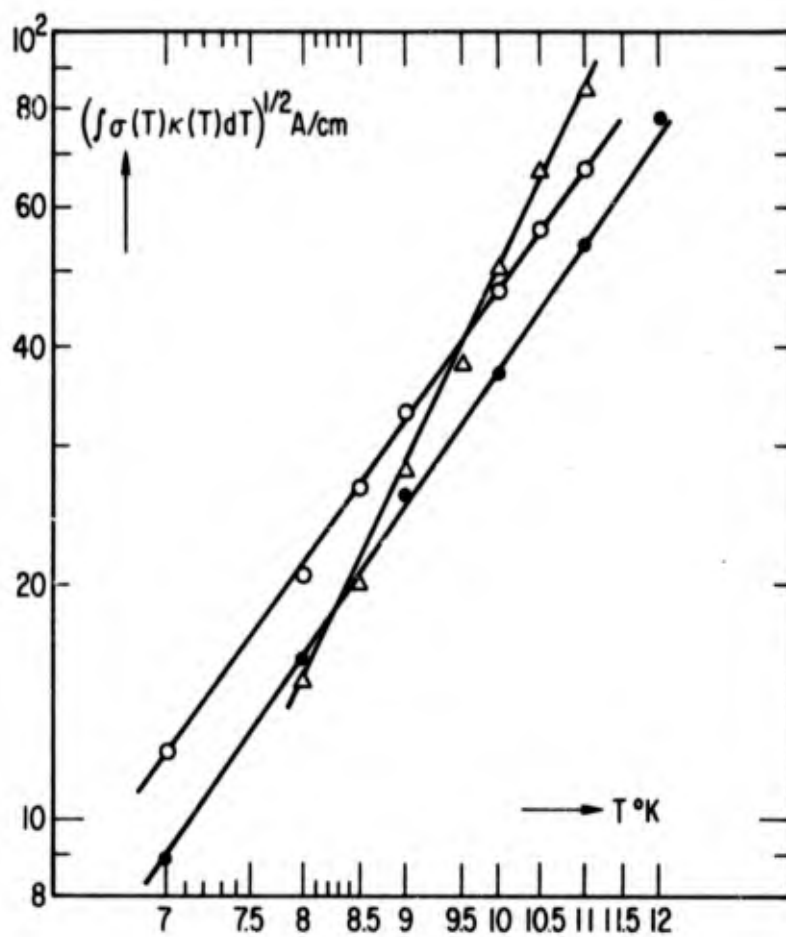


Fig. 15. Variation of temperature integral  $\left[ \int_0^T \sigma(T) \kappa(T) dT \right]^{1/2}$  in A/cm with temperature for argon (●), nitrogen (○), and oxygen Δ[92].

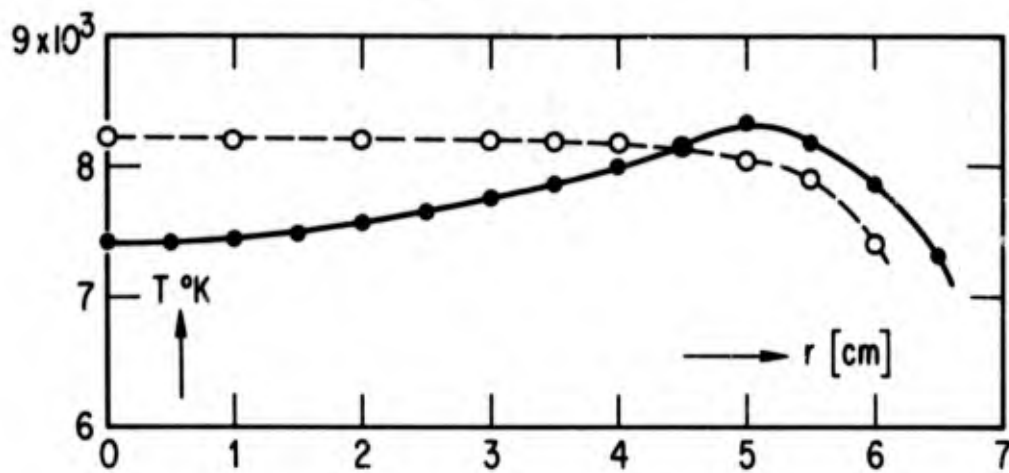


Fig. 16. Comparison between temperatures determined by spectroscopy (—●—) [63] and by magnetic probes (---○---) [35] with the use of Fig. 15.

Freeman and Chase [40], disregarding the radiation term in Eq. (10), adapted the channel model with  $\sigma = \text{const}$  to the induction arc. In order to obtain the additional relationship needed for determination of the channel radius, they invoked Steebeck's principle of minimum entropy production. From this analysis, they concluded that arcs could not exist if their skin depth was less than 0.6 times the channel radius, a result that is contrary to experimental evidence as pointed out in Sec. IIB. Freeman and Chase obtained fair agreement when comparing predicted operating characteristics of arcs in nitrogen, oxygen, and argon with their own experiments.

Gruzdev, Rovinskii, and Sobolev [47, 91, 92], again setting  $Q = 0$ , developed a refined channel model in which the case  $\sigma = \text{const}$  represents the first approximation. By rewriting Eqs. (2) and (3) in terms of  $|E|^2$  and  $|H|^2$ , they reduced the system to one of fifth order, which they integrated, and developed an iteration procedure for the resulting set of integral equations. Data for the channel radius and peak temperature are in satisfactory agreement with the authors' own experiments in argon. They also present calculations of  $|E|$ ,  $|H|$ , and  $j$ , for one example. In work recently reported [93], Rovinskii and Sobolev concluded that the channel model combined with the minimum principle is unsuitable for a qualitative description of an induction arc.

Pridmore-Brown [80, 38], retaining the radiation term, adopted the system of variables from [47] and integrated the equations numerically, treating them as a two-point boundary value problem. He presented distributions of  $T$ ,  $|E|$ , and  $|H|$  for various combinations of  $H_R$ ,  $R$ , and  $\omega$  and also studied the convergence of the solutions. They were found to be very sensitive to conditions at the axis because of the steep rises of  $\sigma$ ,  $\kappa$ , and  $Q$  with  $T$  and to be generally not unique. No widely separated independent solutions were found, however. A comparison of temperature profiles from this theory and experimental data is presented in Fig. 17. The experiments will be discussed in detail in Sec. IIIB.

In addition to these numerical approaches and iteration schemes, some work has also been done on obtaining closed form solutions of the system of Eqs. (2), (3), and (10) by means of simplifying assumptions. Although the results are limited in applicability, they provide some insight into the effects

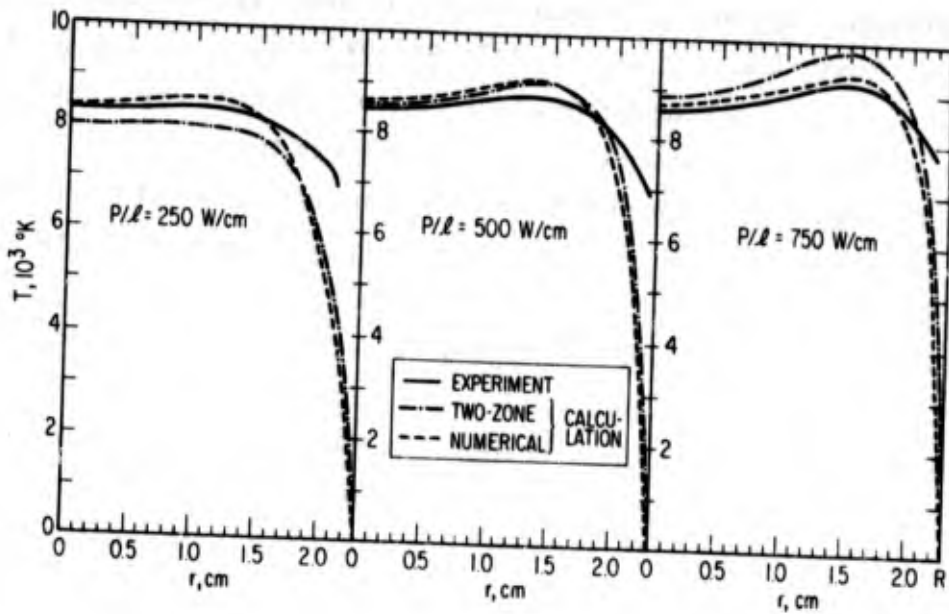


Fig. 17. Comparison between spectroscopically determined temperatures (—) [105], numerical calculations (---) [80], and closed-form solutions by two-zone model (—) [31, 38].

of various parameters that could be obtained through numerical methods only with large expenditure.

This author has developed a two-zone model (not to be confused with the channel model) of the induction arc for cases where radiation losses represent a small, but not negligible, fraction of the input power ( $\sim 10\%$ ) [30, 31]. The energy balance Eq. (10) is linearized with the aid of the heat conduction potential

$$s = \int_0^T \kappa dT \quad (13)$$

and reduces to

$$\frac{d^2 s}{dr^2} + \frac{1}{r} \frac{ds}{dr} + \sigma E^2 - Q = 0 \quad (14)$$

In the outer zone, where most of the heating occurs,  $Q$  may be disregarded against  $\sigma E^2$ . It is assumed that  $\sigma$  varies with  $s$  according to

$$\sigma = c^2 s \quad (15)$$

where  $c^2$  represents the average slope in the  $\sigma(s)$  curve over the range of interest [30, 37]. The variation of  $|E|$  over the radius is approximated by the power law

$$|E| = E_R \left(\frac{r}{R}\right)^q \quad (16)$$

where the exponent  $q$  is close to  $R/\delta$  for  $R/\delta > 2$  [30]. The solution of Eq. (14) for the outer zone can then be written in terms of Bessel functions. If, for simplicity, one sets  $T_R = s_R = 0$ , the result is

$$s = A \left[ J_0 \left[ \lambda \left(\frac{r}{R}\right)^{q+1} \right] - \frac{J_0(\lambda)}{Y_0(\lambda)} Y_0 \left[ \lambda \left(\frac{r}{R}\right)^{q+1} \right] \right] \quad (17)$$

$\lambda$  represents an eigenvalue given by

$$\lambda = \frac{c E_R R}{q+1} \quad (18)$$

At the inner region, the increases in  $Q$  and  $\sigma E^2$  with  $r$  will approximately cancel out; therefore, one may set

$$Q - \sigma E^2 = Q_0 \quad (19)$$

where  $Q_0$  is the value of  $Q$  at  $r = 0$ . In this zone, the solution of Eq. (14) is then given by the parabola

$$s = s_0 + Q_0 \left(\frac{r}{2}\right)^2 \quad (20)$$

In order to obtain a smooth distribution of  $s$  over the radius, one must match the two partial solutions Eqs. (17) and (20) at the zone interface, the location of which depends on the parameters  $\lambda$  and  $q$ . For details of this procedure and determination of the parameters from the input conditions, see Ref. [31].

Comparison of experimental and numerical results is shown in Fig. 17. For a nonradiating plasma, the analysis has also been applied to an arc between coaxial cylinders [37], which essentially means substitution of the interface with the radiation zone by a fixed boundary.

Meierovitch and Pitaevskii [69] have analyzed the heating layer of a nonradiating arc for cases where

$$\delta \ll R \quad (21)$$

so that Eq. (2) reduces to

$$\frac{dE}{dr} = -i\omega\mu H \quad (22)$$

The electric conductivity is assumed to be related to the temperature through

$$\sigma \sim \exp(-I/2T) \quad (23)$$

where  $I$ , the ionization temperature, is considered to be large as compared with  $T_m$ , the maximum temperature in the discharge.

$$T_m \ll I \quad (24)$$

Inside the plasma where  $T \approx T_m$ ,  $\sigma$  is taken as a constant equal to  $\sigma(T_m)$ . Maxwell's Eqs. (2) and (22) are reworked to result in a single fourth order

differential equation for  $|E|^2$ , which, when combined with Eq. (10), yields a fifth order differential equation in T. The following nondimensional expressions for T and r are then introduced

$$T = T_m - \frac{2T_m^2 \theta}{I} \quad (25)$$

and

$$r = - \left( \frac{2}{\sigma_m \mu \omega} \right)^{1/2} \zeta \quad (26)$$

With the substitutions of Eqs. (25), (26), and (23), the equation for T takes the form ( $\kappa = \kappa_m$ )

$$\frac{d^3}{d\zeta^3} e^\theta \frac{d^2 \theta}{d\zeta^2} - e^{-\theta} \frac{d\theta}{d\zeta} = 0 \quad (27)$$

This is a relationship between  $\theta$  and  $\zeta$  without any independent parameters. An asymptotic solution is

$$\theta \sim \exp -(\zeta - \zeta_0) \quad (28)$$

The general solution for Eq. (27) is obtained numerically and, when matched to that for the region  $\zeta_0 > \zeta$ , results in the curve shown in Fig. 18a. The nondimensional energy flux and the energy dissipation obtained from the first and second derivatives of  $\theta$  are shown in Figs. 18b and 18c, respectively.

In a recent paper [71], Meyerovitch has removed the restriction on the skin depth, Eq. (21).

## B. COMPARISON WITH EXPERIMENT, NONEQUILIBRIUM EFFECTS

Results from the earlier experiments permit only a crude, qualitative comparison with predictions from the preceding treatments for one-dimensional, static columns, as the experimenters neither reported the complete input data nor did they try to minimize two-dimensional and convection effects. An exception were the experiments by Stokes [105] who spectroscopically measured

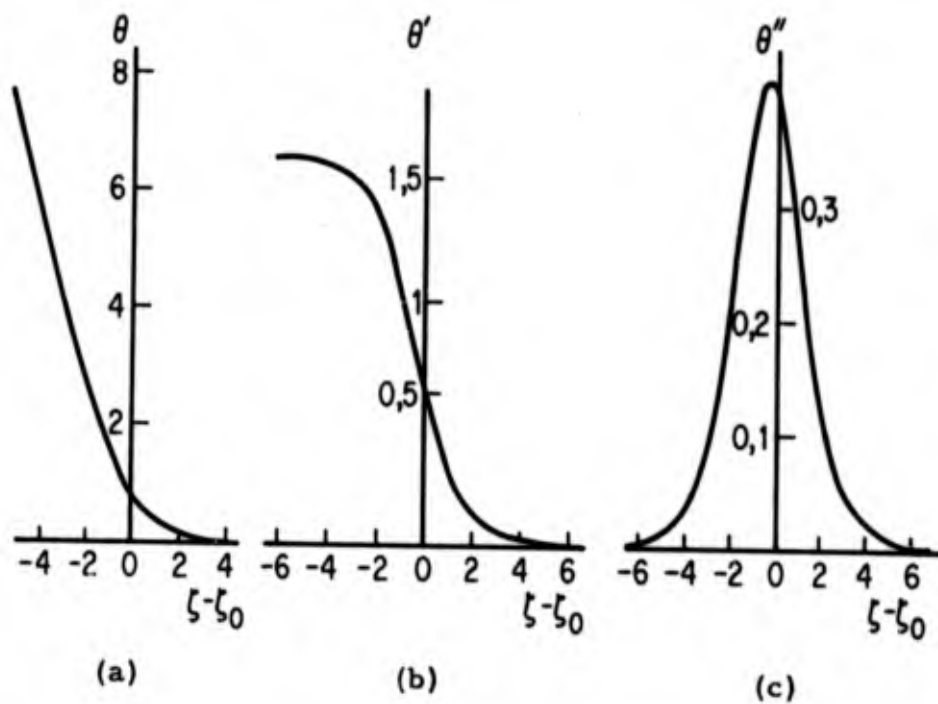


Fig. 18. Results of numerical integration of Eq. (27). (a) Dependence of nondimensional temperature  $\theta$  [defined by Eq. (25)] on nondimensional radial coordinate  $\xi - \xi_0$  ( $\xi - \xi_0 > 0$  inside discharge), (b) nondimensional energy flux  $|\theta'| = I_0 S / 2\kappa T_m$ , and (c) nondimensional heat production  $\theta'' = I_0 r |E^2| / 4\kappa T_m$  [69].

temperatures across the midsection of nearly static, ambient pressure argon columns having five times the length of their diameter. Although he did not report the ampere-turns of the inductor coil, Stokes did measure the rate of dissipation per unit column length  $P/l$ , which represents equivalent information [31, 37]. Temperature profiles for three different values of  $P/l$  have been calculated according to the numerical method of Ref. [80] and the approximate method of Ref. [31]. Details of these calculations are given in Ref. [38]. The results are shown in Fig. 17 with the experimental data. Agreement in the central portion of the profile is generally good, especially for the numerical calculations. It supports the conclusion by Scholz and Anderson [97] and by Trekhov, Fomenko, and Koshev [110] that this portion of the column is in thermal equilibrium. In the outer portion, however, the experimental temperatures show a much slower decline than do the calculated ones. This discrepancy has been interpreted as a nonequilibrium effect [38]. Gradients in electron density caused by the strong temperature gradients near the wall give rise to ambipolar diffusion of electrons and ions and bring the electron concentration above the values corresponding to local Saha equilibrium. Thus, if the Saha equation is used in the reduction of the spectroscopic data, as is common, the temperatures will be too high. This interpretation has been supported by the finding that, in all the profiles measured by Stokes (which also include cases of coaxial geometry), the portions near a wall can be reproduced from a diffusion profile (Bessel function) for the electron concentration [33, 37].

It is thus very likely that not only Stokes but also other spectroscopists have derived excessive temperatures near a confining wall. Conversely, theoreticians have calculated too low temperatures by the use of equilibrium values for  $\sigma$  in this region. With prescribed boundary conditions for  $T_R$  and  $\kappa(dT/dr)_R$ , the latter error is probably less significant and the true plasma temperature can be expected to be closer to the theoretical than to the experimental values. Experiments by Dresvin and Klubnikin [22] with a 32-mm-wide tube confirm the previous findings for low gas flow rates ( $\sim 5$  liters/min). At larger flow rates ( $\sim 20$  liters/min), equilibrium does not even exist at the axis of the column. Whereas the electron temperature slightly

increases with flow rate, the gas temperature decreases sharply. Apparently the collisional exchange between electrons and heavy particles is insufficient to allow the two temperatures to equilibrate. This explains the disagreements between spectroscopically and calorimetrically determined temperatures encountered by some workers [9, 21, 44]. For a large argon plasma flame of 14-cm diam (such as that shown in Fig. 2b), Leonard [63] has found lack of collisional equilibrium over the entire cross section. This does not contradict the findings of equilibrium in the central portion of small diameter columns [97] as electron concentrations in the latter can be higher by an order of magnitude and thus the collisional energy exchange between electrons and heavy particles can be correspondingly closer. A simple empirical relationship between tube radius and average electron density that correlates the majority of experimental data rather well [30] is

$$\bar{n}R \sim 10^{16} \text{ cm}^{-2} \quad (29)$$

### C. TWO-DIMENSIONAL AND CONVECTION EFFECTS, MAGNETIC PUMPING

The condition that all quantities depend on the single space coordinate  $r$  can be verified experimentally over only limited sections of a plasma column. If one wants to analyze the entire column of a real discharge, quantities will necessarily depend also on the axial coordinate  $z$ . An axial velocity  $u_z$  that does not influence conditions in an infinite column will do so in a column of finite length. In addition, there may also exist a radial velocity  $u_r$  due either to the method of gas injection or to magnetic pumping. (This will be discussed later.) Under these generalized conditions, the energy balance equation for a steady-state column has the following form

$$\begin{aligned} \kappa \left( \frac{\partial^2 T}{\partial r^2} + \frac{1}{r} \frac{\partial T}{\partial r} + \frac{\partial^2 T}{\partial z^2} \right) - \rho c_p \left( u_r \frac{\partial T}{\partial r} + u_z \frac{\partial T}{\partial z} \right) \\ + \frac{\partial \kappa}{\partial T} \left[ \left( \frac{\partial T}{\partial r} \right)^2 + \left( \frac{\partial T}{\partial z} \right)^2 \right] + \sigma E^2 - Q = 0 \end{aligned} \quad (30)$$

Miller and Ayen [72] have developed a procedure for the numerical solution of Eq. (30) with  $u_r = 0$  and the boundary conditions

$$T(R, z) = T_{\text{wall}} \quad (31)$$

$$\partial T / \partial r(0, z) = 0 \quad (32)$$

$$T(r, 0) = T_{\text{in}} \quad (33)$$

where  $z = 0$  represents the inlet section upstream of the discharge zone.  $T_{\text{wall}}$  and  $T_{\text{in}}$  are taken as constants. Results of these calculations are shown in Fig. 19 for a discharge geometry and gas flow rate similar to that of Reed [85] at three different power inputs. The two-dimensional temperature distributions exhibit a pattern similar to that obtained experimentally by Goldfarb and Dresvin [42] (Fig. 4). The similarity would have been closer if Miller and Ayen had considered the  $z$ -dependence of  $H_R$  in a finite length induction coil.

If the column is static ( $u_z = 0$ ) and the  $z$ -dependence of variables in Eq. (30) is negligibly small compared with their  $r$ -dependence, particularly if

$$\frac{\partial^2 T}{\partial z^2} \ll \frac{\partial^2 T}{\partial r^2} + \frac{1}{r} \frac{\partial T}{\partial r} \quad \text{and} \quad \left(\frac{\partial T}{\partial z}\right)^2 \ll \left(\frac{\partial T}{\partial r}\right)^2$$

a temperature field can be constructed more simply in a quasi-one-dimensional fashion. The column is divided into a number of discs considered thermally insulated from each other and a  $T(r)$  profile is calculated for each disc that corresponds to the effective value of  $H_R$  at its position  $z$ . These profiles are then cross-plotted into a  $T(r, z)$  map (for an example, see Fig. 20). The analysis of Ref. [31] has been used to calculate the  $T(r)$  profiles. This method becomes inaccurate where  $\partial T / \partial z \sim \partial T / \partial r$  as, for instance, near the axis and at the fringes of the induction coil. If axial heat flux were taken into consideration, the values of  $\partial T / \partial z$  would be lowered.

Raizer [83, 84] has considered a semi-infinite nonradiating column with  $\delta/R \ll 1$  in axial flow. By the use of essentially constant properties, he derives approximate expressions for the temperature variation across the heating layer  $T(x)$  and points out the analogy with the front of a combustion flame. An

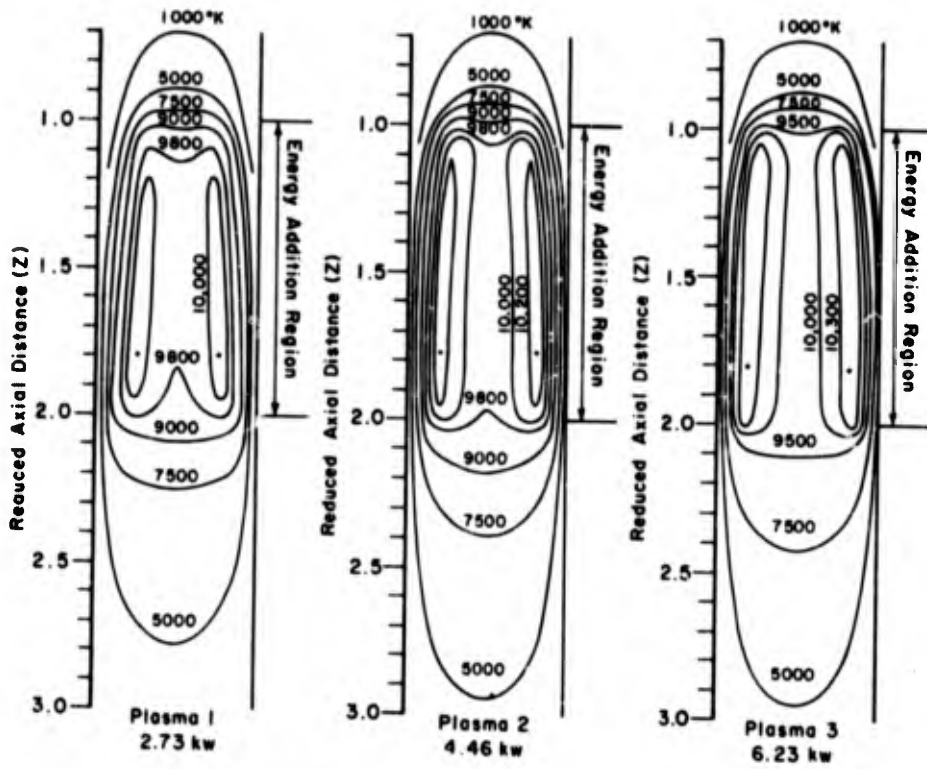


Fig. 19. Computed temperature fields in axial flow for three power levels [72].

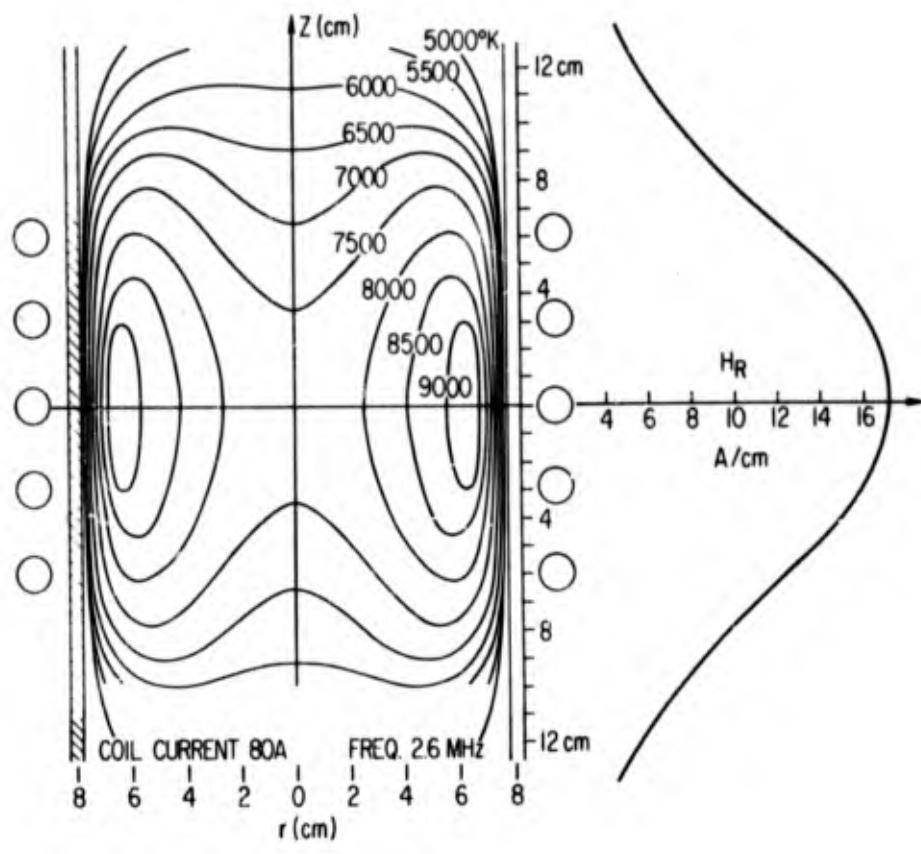


Fig. 20. Temperature field calculated by quasi-one-dimensional approach from axial magnetic field distribution shown at right (see text) ( $f = 2.6$  MHz,  $I_1 = 72$  A,  $u_z = 0$ ).

equation for the maximum temperature  $T_m$  is obtained from a generalized form of Eq. (9), which in our notation reads

$$\int_0^{T_m} \sigma(T) \kappa(T) \left[ 1 + \frac{|\rho_0 u_z| \int_0^{T_m} c_p dT}{T \kappa \frac{dT}{dx}} \right] dT = \frac{H^2 R}{2} \quad (34)$$

Equation (34) is evaluated in an approximate manner, and values of  $T_m$  are tabulated for air and argon flows at various power inputs.

Whereas axial feeding is the most common method, the discharge can also be maintained by an inflow of gas in radial direction. For an example, see Fig. 21. Argon gas is fed from a jacket into the tube through a number of symmetrically arranged holes. Both ends are open to atmosphere and permit axial penetration of the plasma, for instance, by a laser beam. By the injection of the gas through walls of uniform porosity, one can counter the heat flux toward the walls and substantially reduce the conduction losses. If the flow rates are large, the discharge tube will have to be given a conical shape to accommodate the increase in mass flow with  $z$  [29]. Analytically, the case of radial flow into or out of a one-dimensional column can be treated as if an infinite sink or source exists at the axis. Then the approximate method used for solution of the energy equation in the outer zone of the two-zone model [31] can be extended to this case. With the radial convection term added and with  $Q = 0$ , Eq. (14) becomes

$$\frac{d^2 s}{dr^2} + \left( \frac{1}{r} - \frac{\rho u_r c_p}{\kappa} \right) \frac{ds}{dr} + \sigma E^2 = 0 \quad (35)$$

From the continuity of mass flow, it follows that

$$\rho u_r = \rho_R u_R \frac{R}{r} \quad (36)$$

Reproduced from  
best available copy.

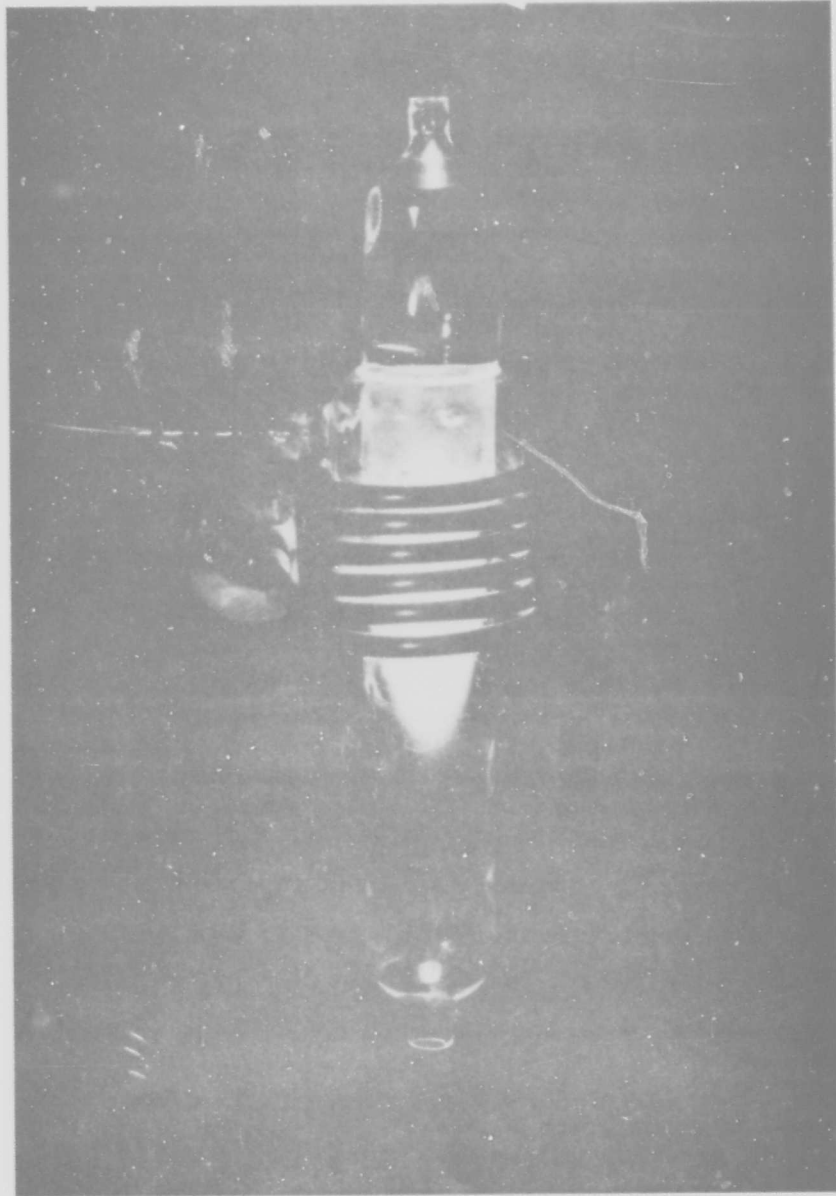


Fig. 21. Induction flame with radial gas supply ( $D = 3.8$  cm).

If one takes  $cp/\kappa$  as a constant, sets

$$\rho_R u_R R \frac{c}{\kappa} \equiv 2b \quad (37)$$

and again uses Eqs. (15) and (16), the solution of Eq. (35) can be written

$$s = \left(\frac{r}{R}\right)^b \frac{Z_b}{q+1} \left[ \lambda \left(\frac{r}{R}\right)^{q+1} \right] \quad (38)$$

where

$$\frac{Z_b}{q+1} = A \frac{J_b}{q+1} + B \frac{Y_b}{q+1} \quad (39)$$

and  $\lambda$  is defined by Eq. (18).

The order of the Bessel function will thus, in general, not be an integer. For  $b = 0$  and  $T_R = 0$ , Eq. (38) reduces to Eq. (17). Because of

$$\frac{\rho}{\rho_R} \approx \frac{T_R}{T} \quad (40)$$

it is not permissible in the general case to use  $T_R = 0$  as a boundary condition.

A small radial inflow exists also in an ordinary induction column because of "magnetic pumping." The rf magnetic field superimposes a slight magnetic pressure  $\mu H^2/2$  on the kinetic pressure  $p$  in the plasma. Except for viscosity effects, which are disregarded, the total pressure in the plasma will be a constant or

$$\frac{d}{dr} \left( \mu \frac{H^2}{2} + p \right) = 0 \quad (41)$$

As  $H$  decreases toward the axis, especially in the skin layer,  $p$  must increase according to Eq. (41). Because of the magnetic pressure gradient, electrons and ions drift toward the center and transmit their motion by momentum exchange to the neutral particles. For a finite length coil, this action will be strongest at the midsection where the magnetic field has its maximum. At this

section, the flow will stagnate and be diverted axially toward both ends of the coil. From there it will return to the outer boundary and form a double vortex system that may be superimposed to an axial flow. This is shown schematically in Fig. 22, which is adopted from Chase [13]. He was the first to draw attention to the magnetic pinch in an induction arc [12], to measure the pressure rise with a sensitive manometer, and to demonstrate the existence of axial outflow by the reflection of light particles dropped onto the flame, as shown by the photographs in Fig. 23. Dymshits and Koretski [28] have calculated the axial acceleration of plasma due to radial components of  $H$  near the ends of the column and obtained velocities around 10 m/sec. This agrees by order of magnitude with the measurements of Chase [13]. Much of this magnetic axial force probably accounts for the phenomena in Fig. 23.

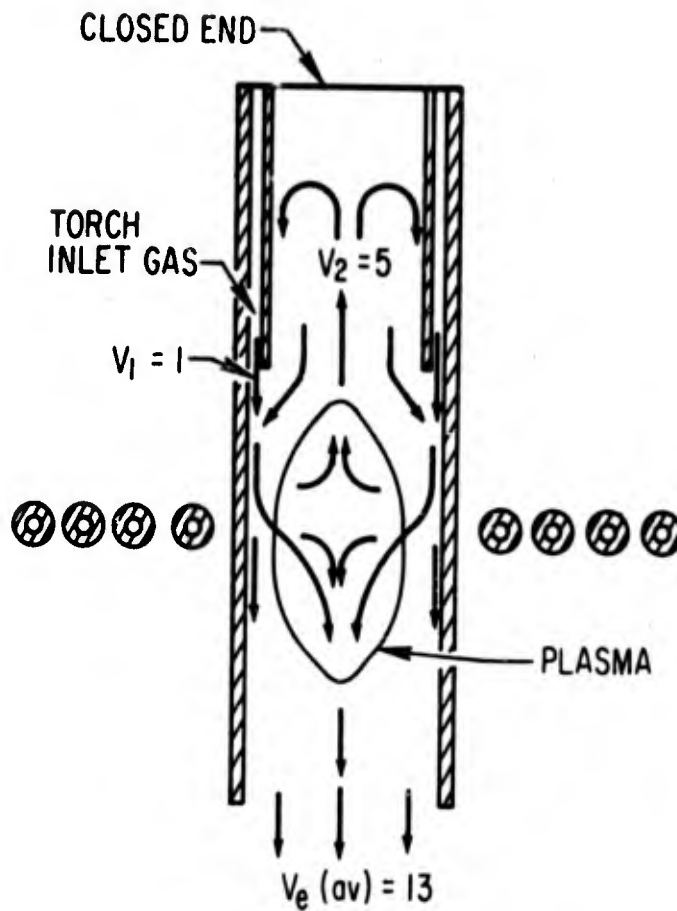
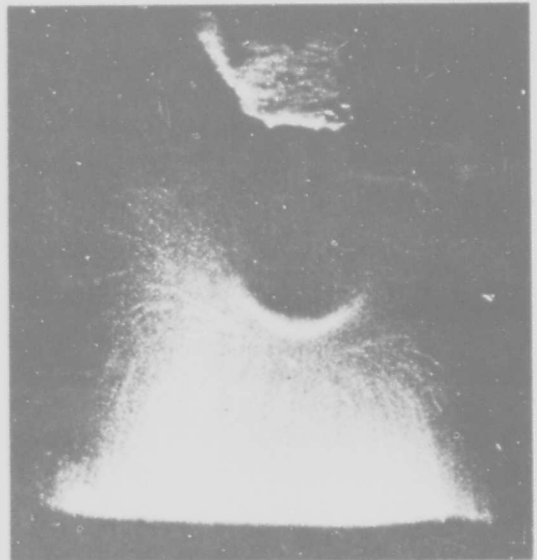


Fig. 22. Flow pattern and velocities (m/sec) in induction flame [13] ( $D = 2.8$  cm,  $P = 2.5$  kW).

Reproduced from  
best available copy. 



(a)  $P = 1.5 \text{ kW}$



(b)  $P = 5 \text{ kW}$

Fig. 23. Reflection of  $10\mu$  alumina particles from top of induction flame [13].

#### IV. APPLICATIONS

The absence of electrodes makes the induction arc suited for a variety of scientific and engineering applications. It has the following advantages:

1. Production of clean plasmas
2. No life limitation due to electrode erosion
3. Reduced heat conduction losses
4. Unobstructed cross section.

Item 1 is especially important because it applies not only to noble gases but also to the reacting molecular gases. As to the physical applications, we have seen in Sec. IIIB that, with the proper choice of conditions, the bulk of the plasma is in, or near to, thermal equilibrium. If this holds for argon, it can be expected to hold even closer for molecular gases because of the increased frequency of inelastic electron collisions. This makes the induction arc suitable for determination of transport properties of arbitrary gases and vapors. Correlation of the properties with independent temperature measurements enables one to check the predictions from an equilibrium theory. As an example, Fig. 24 shows a comparison of the argon electric conductivity derived from the double probe measurements in [36] and the calculated data. Also shown are results from shock tube and dc arc measurements. In [36], commercial argon was used. For methods to reduce the impurity level of this gas, see Ref. [18].

Several authors have derived values for the electron-ion recombination coefficient in atmospheric argon defined by

$$\frac{dn}{dt} = -\alpha n^2 \quad (42)$$

A crude estimate was made in [111] that yielded  $\alpha \sim 10^{-12} \text{ cm}^3/\text{sec}$  for  $T \sim 10000^\circ \text{K}$ . Superimposing a magnetic pulse on the rf plasma, Shamin and Wooding [91] determined  $dn/dt$  and  $n$  at the axis via the Saha equation from temperature measurements in the pulse decay phase. For  $n \sim 4 \times 10^{16}$  and  $T \sim 11000^\circ \text{K}$ , they obtained  $\approx 3.4 \times 10^{-14} \text{ cm}^3/\text{sec}$ . Desai and Corcoran [18]

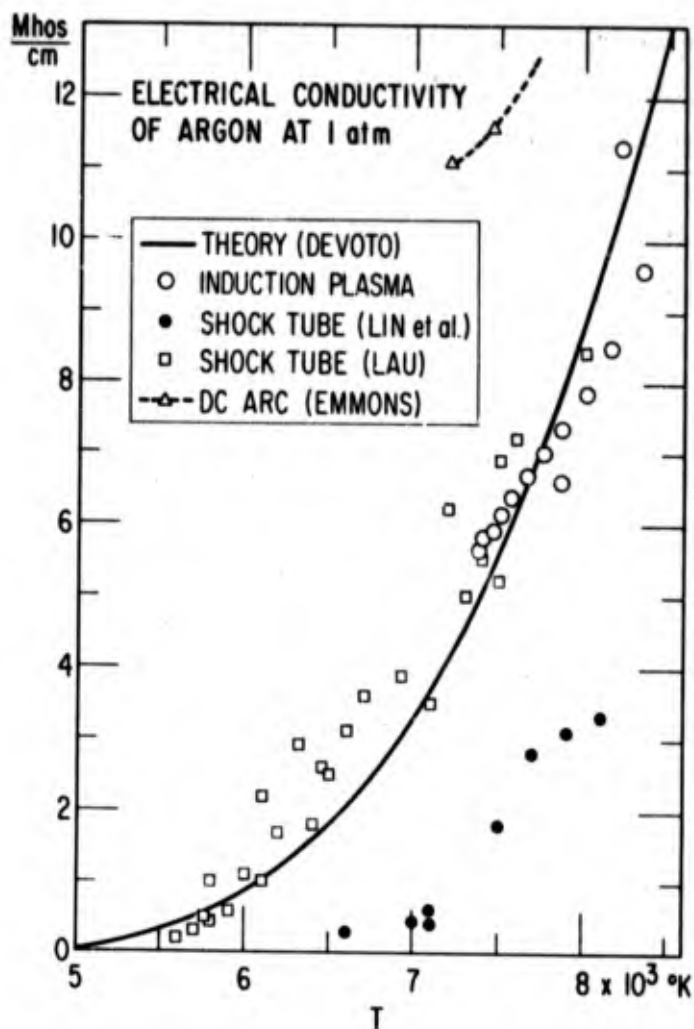


Fig. 24. Correlation of electric conductivity data of Fig. 11 with equilibrium temperatures and comparison with results of other investigators [36].

determined  $\alpha$  for ranges of  $n$  between  $10^{12}$  and  $10^{15}$   $\text{cm}^{-3}$  and of  $T$  between  $3000^\circ$  and  $11000^\circ\text{K}$ , where it fits the relationship

$$\alpha = 1.28 \times 10^5 T^{-1.8} \times 10^{\frac{-3410}{T}} n^{-0.64} \quad (43)$$

This form of dependence, where  $\alpha$  decreases with increasing  $n$ , cannot be explained by a radiative-collisive process and suggests a process by dissociation of  $\text{A}_2^+$  ions. Stokes [106], from measurements between  $n = 3 \times 10^{14}/\text{cm}^3$  and  $2 \times 10^{15}/\text{cm}^3$  and  $T_e$  between  $5500$  and  $9000^\circ\text{K}$  at  $p = 76$  Torr, derived the simpler formula

$$\alpha = \frac{2700}{n} \quad (44)$$

In another experiment, Hughes, Shamin, and Wooding [55] obtained  $\alpha \sim 5 \times 10^{-13} \text{cm}^3 \text{sec}^{-1}$  for  $n \sim 2 \times 10^{15} \text{cm}^{-3}$ . In the later phases of the decaying pulse, ambipolar diffusion is the dominating electron loss process. For the ambipolar diffusion coefficient, the authors obtain  $\text{Da} \sim 500 \text{cm}^2 \text{sec}^{-1}$ . Malone and Corcoran [66] and Desai and Corcoran [16, 17] have used induction arcs for determining transition probabilities of numerous AI lines in the visible regime.

Several workers have investigated the suitability of the argon induction arc for spectral chemical analysis. Wendt and Fassel [119] have combined the torch with an aerosol generator and presented emission detection limits for 20 elements in aqueous solutions ranging from  $0.09 \mu\text{g}/\text{ml}$  for strontium to  $50 \mu\text{g}/\text{ml}$  for tin. Similar investigations, including absorption tests, were made by Veillon and Margoshes [112]. The authors found the induction torch helpful for detection of refractory elements but, because of its higher cost, generally not a suitable replacement for a chemical flame. Kleinmann and Cajko [60] made a thorough spectroscopic analysis of an unusually small argon flame ( $D = 1.3 \text{cm}$ ,  $P \sim 200 \text{W}$ ,  $f = 50 \text{MHz}$ ) with various introduced impurities. The plasma is found to be in strong disequilibrium ( $T_a \sim T_{\text{mol}} = 2000^\circ\text{K}$ ,  $T_{\text{exc}} \approx 4400^\circ\text{K}$ ,  $T_e = 11400^\circ\text{K}$ ,  $n \approx 4 \times 10^{14} \text{cm}^{-3}$ ). Comparison of radial intensity distributions of GaI and SrI lines with similar excitation potentials shows that the heavier strontium is more concentrated near the axis,

which indicates a slower diffusion rate. The authors conclude that the high intensity and narrow width of the spectral lines, combined with the low background continuum, make the induction flame a suitable device for spectral analysis, preferably for materials requiring high detection power, and also for isotopic analysis.

Turning now to more practical applications, we recall that Reed, soon after his first publication on the induction torch [86], described how this device can be used to grow crystals [79] from powdered refractory materials such as sapphire, zirconia, and niobium. Other workers [20, 14] have further developed the method and extended it to various materials. A diagram of the apparatus used by Chase and van Ruyven [14] is shown in Fig. 25. A related application is the spheroidization of micron to millimeter size particles as first described by Hedger and Hall [48].

Several authors have investigated, either by analysis [52, 54] or experiment [82], the suitability of induction plasmas for aerodynamic testing under reentry conditions. Vermeulen, Boddie, and Wierum [113] superimposed induction heating to a dc plasma jet to enhance thrust and to obtain a more uniform temperature distribution. Other applications are concerned with simulation of a nuclear plasma to be used in a rocket engine [79, 89, 114, 115, 116]. Related studies have been carried out on plasmas seeded with heavy metals (W, U) to enhance their opacity [7, 90].

The good radiation efficiency of high pressure induction plasmas mentioned in Sec. IID makes promising the development of a high intensity light source with considerably longer life expectancy than present electrode lamps. An example is shown in Fig. 26. The inductor coil may be given a shape suitable for a reflector.

Perhaps the most important application of induction plasmas, which is only in the first stage of exploration, is in chemical synthesis. We refer to the comprehensive article by Vurzel and Polak on plasma chemical technology [117]. Leprince-Ringuet, et al., [64] produced refractories, such as ZrC, ZrN, and several oxynitrides of Al, either in solid-solid or solid-gas phase reactions. In the first case, the plasma consisted of pure argon and served as a

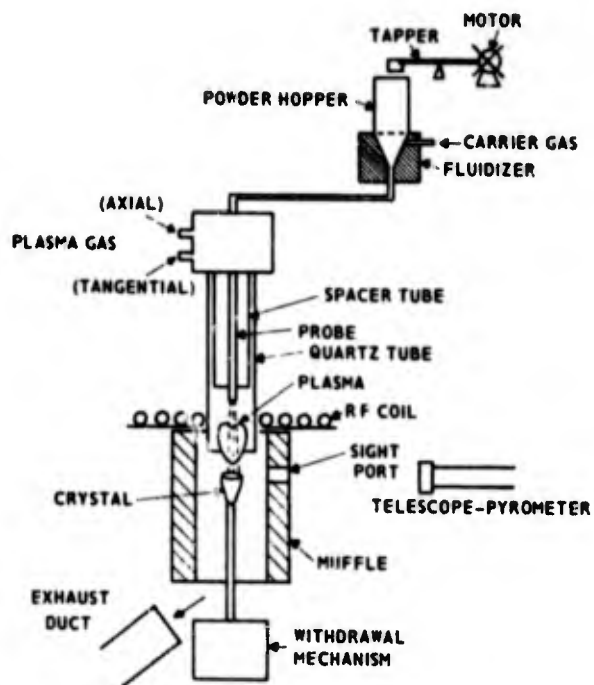


Fig. 25. Schematic diagram of apparatus for crystal growth<sup>[14]</sup>.

Reproduced from  
best available copy.

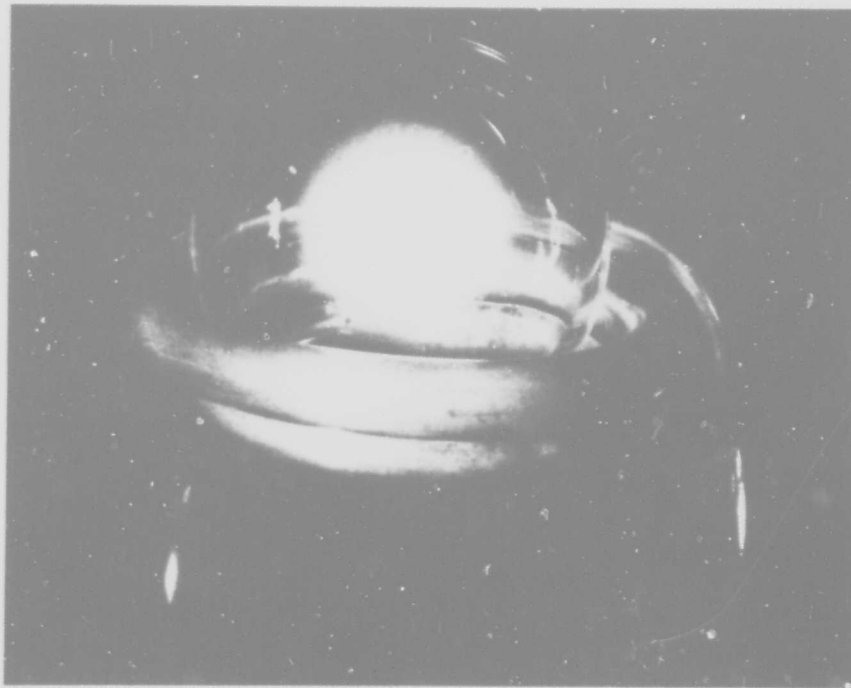


Fig. 26. Electrodeless lamp in spherical quartz enclosure  
(argon,  $p \sim 2$  atm,  $P \sim 300-400$  W,  $D = 3.7$  cm)  
(Courtesy Charybdis Corporation,  
Anaheim, California).

heat transfer agent only. In the latter case, it consisted of argon-nitrogen mixtures. The synthesis of hydrogen cyanide from methane and nitrogen in an induction torch with argon as a diluent has been studied by Bronfin [10]. Rapid quenching resulted in yields of HCN, expressed as a fraction of the nitrogen input converted, of up to 70%. See also [107] on this reaction. Experiments on oxydation of nitrogen and preparation of chlorofluorocarbons are described by Beguin, et al. [4]. Although the yields obtained in these reactions are generally encouraging, large-scale industrial production is hampered by the expenditure for intermediate power-conditioning equipment and the rather low conversion efficiency of conventional high-frequency induction arcs. Often the efficiency does not exceed 50% when auxiliary power requirements, such as tube filament heating, are included. It is important, therefore, to investigate the possibility of more direct conversion of electric power into plasma heat, while retaining the advantages of the electrodeless arc. The basic requirement is that the maintenance voltage of the arc  $V$  can be generated in a single turn. Because

$$|V| = \pi R^2 \mu \omega H \quad (45)$$

it is evident that one can trade between  $\mu$  and  $\omega$  and produce the same  $V$  by lowering  $\omega$  from the megaHertz to the kiloHertz regime and using a magnetic material with  $\mu \sim 10^3 \mu_0$ . At these frequencies, motor-generators that are more economical than vacuum tube oscillators can be used. In order to have good coupling at the reduced frequencies, it is essential that the magnetic material form a closed path for the flux as in an ordinary transformer. It is then necessary to change the plasma vessel from cylindrical to toroidal geometry. A low-pressure glow discharge maintained in such a geometry at  $f = 9600$  Hz is shown in Fig. 27, and an arc obtained by raising the pressure is shown in Fig. 28. The cross section of the iron core is  $100 \text{ cm}^2$ . For details, see Ref. [34].

After the maximum possible flux density  $\mu H$  is obtained,  $\omega$  can be further lowered by increasing the core cross section  $\pi R^2$  until such a "plasma transformer" can be operated at 60 Hz directly from the power line. This would eliminate all intermediate equipment. Shown in Fig. 29 are the variations of

Reproduced from  
best available copy.

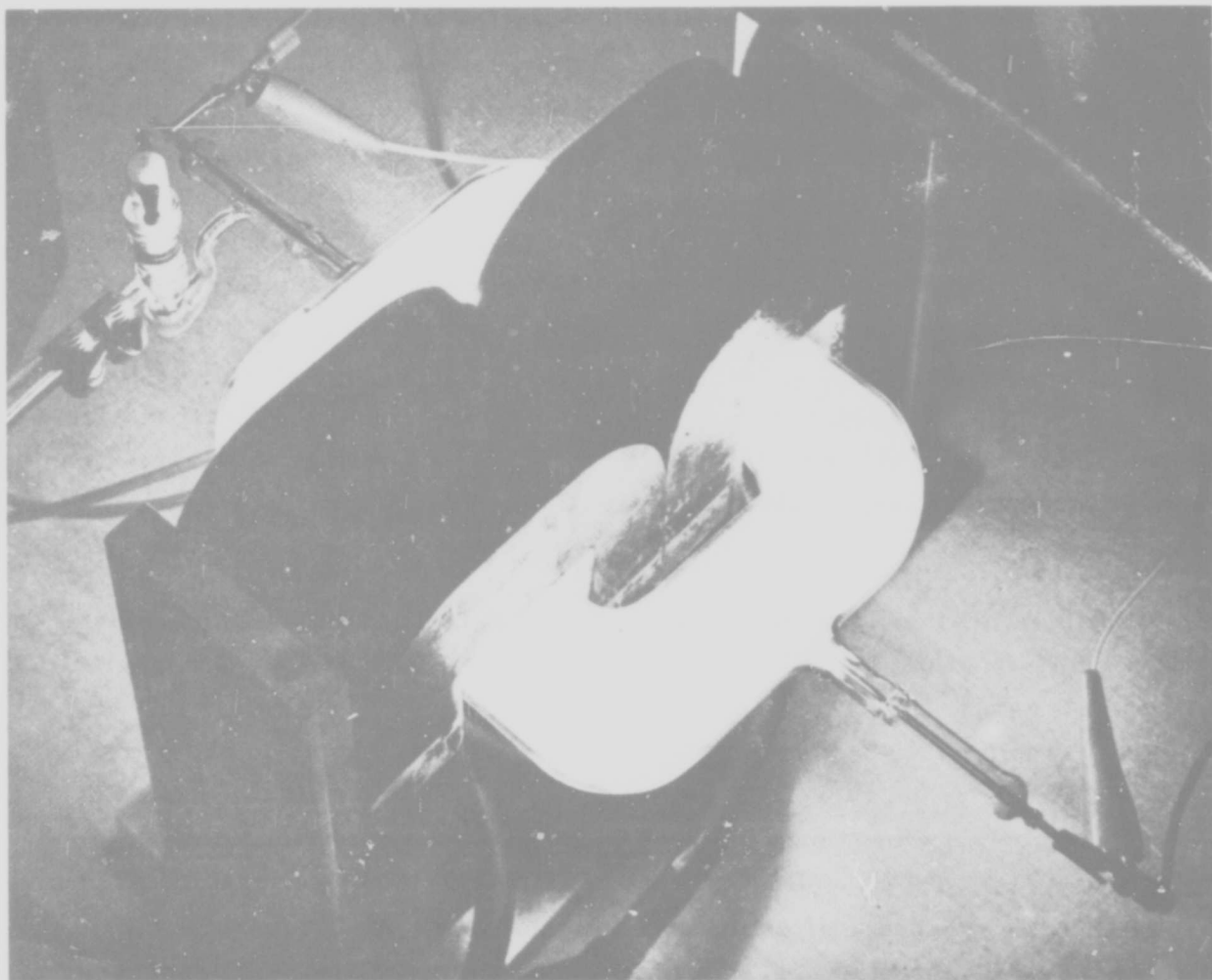


Fig. 27. Starting phase of low frequency electrodeless arc in argon ( $p \sim 0.1$  Torr,  $f = 9600$  Hz,  $V_2 \approx 15$  V,  $I_2 = 150$  A) [34].

Reproduced from  
best available copy.

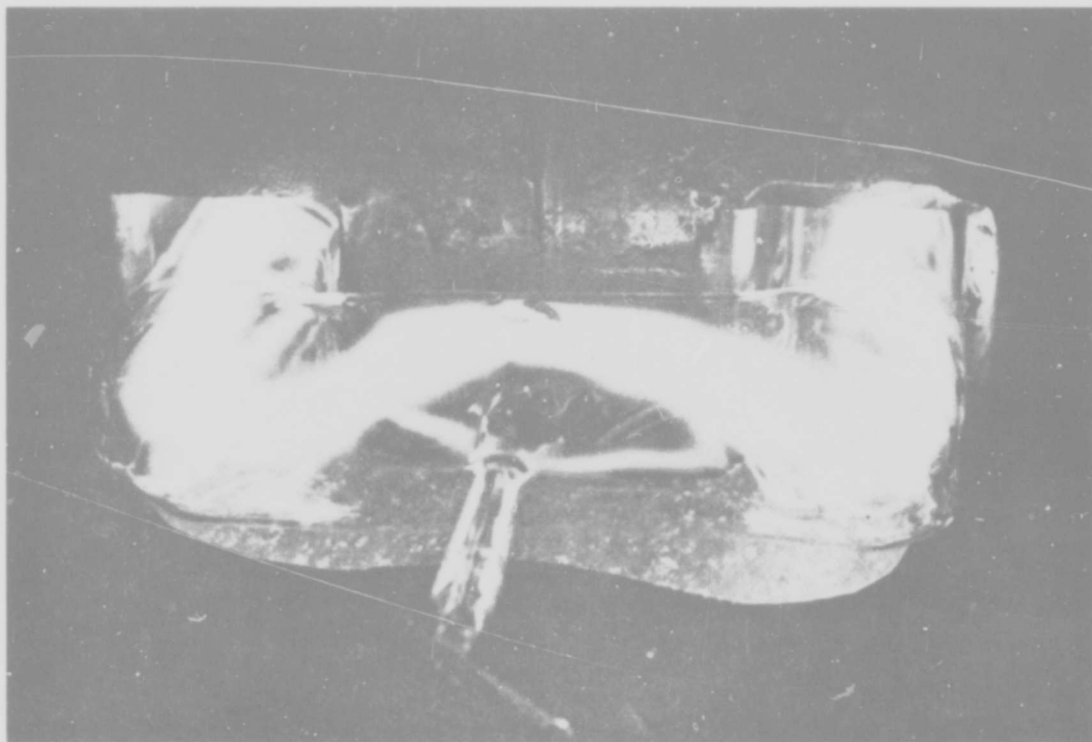


Fig. 28. Inductive electrodeless arc in argon ( $p \approx 400$  Torr,  
 $f = 9600$  Hz,  $V_2 \approx 120$  V,  $I_2 \approx 105$  A) [34].

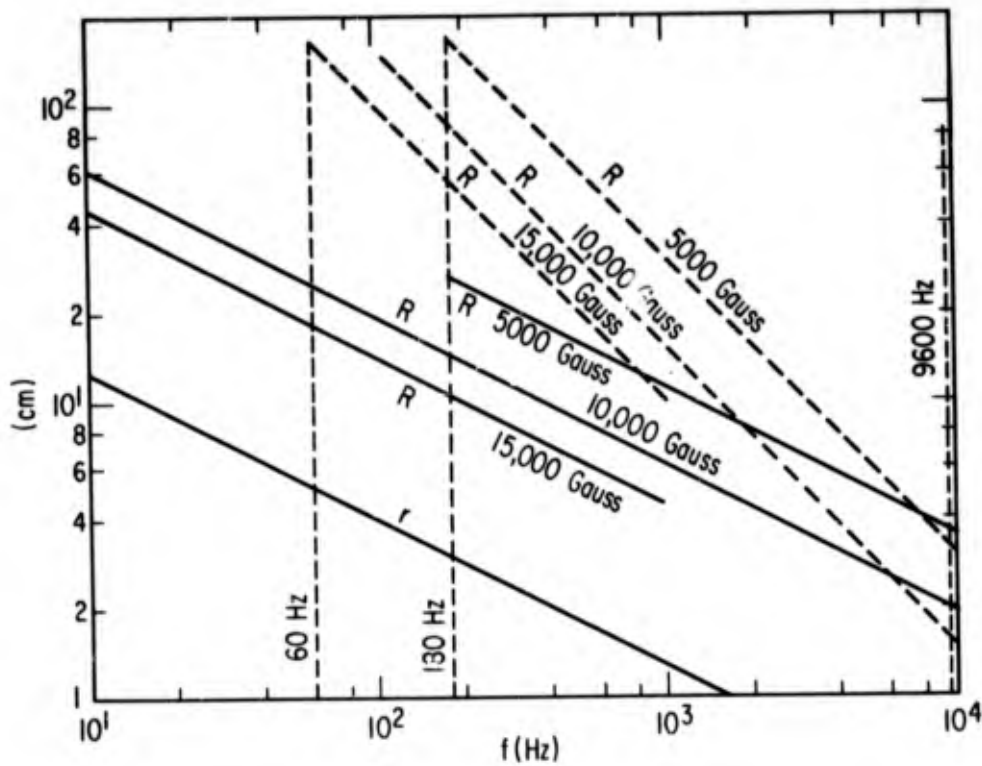


Fig. 29. Minimum values of magnetic core radius  $R$  and tube radius  $r$  for maintaining electrodeless arc in argon at  $p = 1$  atm for several magnetic flux densities [34].  
 [Arc attached to tube wall (—); arc separated from tube wall (- - -)].

the core radius  $R$  and of the tube radius  $r$  (minimum  $r$  required to keep plasma in quasi-steady state [34] ) with frequency  $f$  for several flux densities at two limiting cases. The lower values hold for the condition that the arc is attached to the tube wall, in which case  $V$  is independent of  $f$  for constant  $R/r$ . Therefore,  $R \sim f^{-1/2}$  according to Eq. (45). The upper values hold for the condition where the arc is separated, in which case  $V \sim R + r$  and  $R \sim f^{-1}$ . The frequency  $f = 180$  Hz shown beside the  $f = 60$  Hz line is encountered in the conversion of 3-phase, 60-Hz power into single-phase power. The power required for these two cases diverges even more with  $f^{-1}$  than does the size of the equipment. For 60 Hz, it varies from about 25 kW for the attached arc to about 10 MW for the separated arc. As many reactions have been performed in glow discharges where the plasma is attached, one can expect the lower figure to be more realistic, even though no allowance has been made for the voltage increment required to compensate for the heat going into an endothermic reaction. Because the efficiency of a well-designed transformer is better than 90%, the low frequency induction arc would be the most efficient device for converting electric power into plasma and, thus, to make plasma chemistry economically attractive.

## V. SUMMARY AND CONCLUSIONS

Theory, experimental techniques, and applications of the rf induction arc, which have advanced considerably over the past ten years, are reviewed. Stability considerations and experience indicate that this arc has natural stability only if the ratio of plasma radius to skin depth exceeds 1.75. In theoretical treatments the heat balance equation is solved simultaneously with Maxwell's equations generally for a static, one-dimensional plasma column in thermal equilibrium. Numerical, as well as approximate, analytical methods for solution have been developed and applied to columns in argon or air at atmospheric pressure. The radial temperature profiles show an off-axis maximum that results from the combination of skin heating and radiation cooling. A considerable amount of experimental data on temperature in atmospheric argon arcs is available that has been derived from spectroscopic measurements on the assumption of Saha equilibrium. Maximum temperatures range between about 8000 and 11000°K and are generally higher for the smaller arcs. Quantitative comparison with theoretical data has only recently become possible, when complete input conditions were reported for the experiments. It is found that, for the common discharge tube diameters of a few cm and supply gas velocities of less than 1 m/sec, the plasma core is practically in thermal equilibrium, but the skin layer has an excess electron concentration that is probably caused by ambipolar diffusion to the wall. Lack of equilibrium in the center has been found for very small, as well as for very large, argon discharges and also for large gas supply rates. A few attempts have been made to include effects of axial or radial convection into the heat balance. Small but measurable self-magnetic forces drive the plasma inward at the sides and outward at the ends of the column, which superimposes a double vortex system onto the general flow. In a dc magnetic field, the plasma displays slightly paramagnetic or diamagnetic behavior, depending on the field strength. In closed, thick-walled vessels, induction arcs have been maintained at pressure up to 40 atm. At these pressures, most of the electrical input leaves the plasma in the form of optical radiation, which makes the development of an efficient high intensity light source

promising. Next to spectroscopy, probing of the plasma by miniature coils has become an important diagnostic method and has furnished information about fields, induced current, and electric conductivity. The absence of contamination by electrode material makes the induction arc suitable for applications where a clean plasma is essential. It has been used to determine physical properties of gases, to detect trace elements in spectro-chemical analysis, to grow crystals of refractory materials, and to spheroidize small particles. The most important application may be in the field of chemical synthesis, which so far has been limited to laboratory experiments. If this field is to become economically more attractive, the development of low frequency arcs, which are coupled to the primary coil by a closed iron path and which in sufficiently scaled-up devices may operate at frequencies as low as 60 Hz, appears essential. Other efforts should be directed to generation of induction arcs in reactive gases, such as oxygen or chlorine, where the advantage of the electrodeless principle is most obvious. In order to broaden the theoretical base, it would be desirable to include the electron energy and the electron continuity equation into the system of equations for treatment of nonequilibrium effects. Also, a stability analysis that includes gas properties and convection would prove valuable to the experimenter. As the working principles of the induction arc become better understood, less effort will be expended on methods of application.

## REFERENCES

1. D. R. Armstrong and W. E. Ranz, "Design of Inductively Coupled Plasma," Ind. Eng. Chem., Process Des., and Develop. 7, 31-33 (1968).
2. P. A. Arsen'ev and E. F. Kustov, "Investigation of a High-Frequency Gas Discharge," Teplofiz. Vys. Temp. 6, 44-47 (1968).
3. G. I. Babat, "Electrodeless Discharges and Some Allied Problems," J. Inst. Elec. Engrs. (London) 94, 27-37 (1947).
4. C. P. Beguin, et al., "Chemical Synthesis in Radio-Frequency Plasma Torches," pp. 35-53 in The Application of Plasmas to Chemical Processing, ed. R. F. Baddour and R. S. Timmins, The MIT Press, Cambridge, Mass. (1967).
5. L. E. Belousova, "Relation of Radius to Power for a Thermal Plasma of Spherical Shape," Teplofiz. Vys. Temp. 4, 499-502 (1966).
6. L. E. Belousova, "Thermal Plasma Radius as a Function of Power, Allowing for the Effect of the Wall," Teplofiz. Vys. Temp. 5, 1113-1114 (1967).
7. R. A. Benns, et al., "Measurement of Seeded Argon-Hydrogen Plasma Properties," Paper presented 2nd Symposium Uranium Plasmas: Research and Applications, Atlanta, Ga., November 15-17, 1971, Collection of papers, 150-155.
8. J. Besombes-Vailhe, "Etude de la Repartition de la Temperature Moyenne dans le Jet d'une Torche a Plasma d'Argon Haute Frequence," J. Chim. Phys. 64, 370-376 (1965).
9. J. Besombes-Vailhe, "Etudes par des Methodes Calorimetrique d'une Decharge Haute Frequence dans l'Argon a la Pression Atmospherique," Rev. Phys. Appl. 2, 225-233 (1967).
10. B. R. Bronfin, "Hydrogen Cyanide Synthesis in a Thermal Radiofrequency Induction Plasma " in Chemical Reactions in Electrical Discharges, ed. B. D. Blaustein, Advan. Chem. Seri. 80, 423-440 (1969).
11. Yu. A. Buevich, et al., "Optical Properties of a Plasma from an Electrodeless Discharge in an Air Stream," Zh. Prikl. Mekhan. Tekh. Fiz. 6, 111-116 (1968).

12. J. D. Chase, "Magnetic Pinch Effect in the Thermal RF Induction Plasma," J. Appl. Phys. 40, 318-325 (1969).
13. J. D. Chase, "Theoretical and Experimental Investigation of Pressure and Flow in Induction Plasma," J. Appl. Phys. 42, 4870-4879 (1971).
14. J. D. Chase and L. V. van Ruyven, "Plasma Grown Rutile Single Crystals and their Distinctive Properties," J. Cryst. Growth 5, 294-298 (1969).
15. M. Clement, et al. "Experimental Study of an RF Argon Torch," Proc. VIe Conf. Internatl. sur les Phenom. d'Ionization dans les gas, II, 505-508, Paris (1963).
16. S. V. Desai and W. H. Corcoran, "Some New Transition Probabilities of Argon I in the Range of 5000-6500 A and the role of a Nonuniform Source Temperature," J. Quant. Spectrosc. Radiat. Trans. 6, 443-449 (1966).
17. S. V. Desai and W. H. Corcoran, "Improved and Corrected Transition Probabilities of Argon I in the Range of 5000-6000 A," J. Quant. Spectrosc. Radiat. Trans. 9, 1489-1491 (1969).
18. S. V. Desai and W. H. Corcoran, "Recombination of Electrons and Ions in an Atmospheric Argon Plasma," J. Quant. Spectrosc. Radiat. Trans. 9, 1371-1386 (1969).
19. A. V. Donskoi, S. F. Dresvin, and D. G. Ratnikow, "High Frequency Induction Discharge in a Chamber with Watercooled Metal Walls," Teplofiz. Vys. Temp. 3, 922-923 (1965).
20. A. V. Donskoi, et al., "Some Features of the Processes of Growth of Refracting Crystals in High Frequency Plasma Torches," Teplofiz. Vys. Temp. 3, 627-631 (1965).
21. S. V. Dresvin, A. B. Donskoi, and V. M. Goldfarb, "Determination of the Conductivity of a High Frequency Induction Discharge by Calorimetric and Spectral Methods," Zh. Tekh. Fiz. 35, 1646-1651 (1965).
22. S. V. Dresvin and V. S. Klubnikin, "Disequilibrium in an Argon Plasma Jet from a High-Frequency Induction Discharge at Atmospheric Pressure," Teplofiz. Vys. Temp. 9, 475-482 (1971).
23. P. H. Dundas and M. L. Thorpe, "Economics and Technology of Chemical Processing with Electric Field Plasmas," Chem. Eng., 123-128 (June 30, 1969).

24. P. H. Dundas and M. L. Thorpe, "Titanium Dioxide Production by Plasma Processing," Chem. Eng. Progr. 66, 66-71 (1970).
25. P. H. Dundas, Induction Plasma Heating: Measurement of Gas Concentrations, Temperatures and Stagnation Heads in a Binary Plasma System, NASA Contract. Rept. CR1527 (February 1970).
26. R. H. Dundas, "Low Frequency Induction of Thermal Plasma," Paper presented Tenth Internl. Conf. Phen. Ion. Gas., Oxford, England, 1971, Contrib. Papers, p. 243.
27. B. M. Dymshits and Ya. P. Koretskii, "An Experimental Investigation of Induced Discharges," Zh. Tekh. Fiz. 34, 1677-1682 (1964).
28. B. M. Dymshits and Ya. P. Koretskii, "Evaluation of the Effect of Electromagnetic Forces on the Channel of a Constricted Induction Discharge," Zh. Tekh. Fiz. 39, 1039-1043 (1969).
29. H. U. Eckert, Transpiration Cooled Electrodeless Plasma Generator and Accelerator. U. S. Pat. 3,343,022 (19 September 1967).
30. H. U. Eckert, "Analysis of Thermal Induction Plasmas Dominated by Radial Conduction Losses," J. Appl. Phys. 41, 1520-1528 (1970).
31. H. U. Eckert, "Analytical Treatment of Radiation and Conduction Losses in Thermal Induction Plasmas," J. Appl. Phys. 41, 1529-1537 (1970).
32. H. U. Eckert, "Direct Measurement of the Maintenance Voltage of a Thermal Induction Plasma," J. Appl. Phys. 41, 3633-3637 (1970).
33. H. U. Eckert, "Effect of Electron Diffusion on Gas Temperature Measurements in Induction Plasmas," Paper presented Tenth Internatl. Conf. Phen. Ion. Gas., Oxford, England, 1971, Contrib. Papers, p. 244.
34. H. U. Eckert, "Induction Plasmas at Low Frequencies," AIAA J. 9, 1452-1456 (1971).
35. H. U. Eckert, "Measurement of the Magnetic Field Distribution in a Thermal Induction Plasma," J. Appl. Phys. 42, 3108-3113 (1971).
36. H. U. Eckert, "A Dual Magnetic Probe System for Phase Measurements in Thermal Induction Plasmas," J. Appl. Phys. 43, 2707-2713 (1972).
37. H. U. Eckert, "Analysis of Thermal Induction Plasmas between Coaxial Cylinders," J. Appl. Phys. 43, 46-52 (1972).

38. H. U. Eckert and D. C. Pridmore-Brown, "Temperature Profiles in Argon Induction Plasmas: Theory and Experiment," J. Appl. Phys. 42, 5051-5054 (1971).
39. H. U. Eckert, F. L. Kelly, and H. N. Olsen, "Spectroscopic Investigations on Induction Coupled Plasma Flames in Air and Argon," J. Appl. Phys. 39 (3), 1846-1852 (1968).
40. M. P. Freeman and J. D. Chase, "Energy-Transfer Mechanism and Typical Operating Characteristics for the Thermal RF Plasma Generator," J. Appl. Phys. 39, 180-190 (1968).
41. F. Galtier, et al., "Sur le Chalumeau a Plasma Haute Frequence," C. R. Acad. Sci. Paris, Ser. B 255, No. 20, 2539-2541 (1962).
42. V. M. Goldfarb and S. V. Dresvin, "Optical Investigation of the Distribution of Temperature and Electron Density in an Argon Plasma," Teplofiz. Vys. Temp. 3, 333-339 (1965).
43. V. M. Goldfarb and V. Kh. Goikhsman, "Characteristics and Possible Spectroscopic Applications of the High-Frequency Discharge at Atmospheric Pressure," Zh. Prikl. Spektrosk. 8, 193-196 (1968).
44. V. M. Goldfarb, et al., "Investigation of Plasma Torch of High Frequency Argon Burner," Teplofiz. Vys. Temp. 5, 549-556 (1967).
45. V. A. Gruzdev, "Characteristics of an Electrodeless Discharge in Xenon," Teplofiz. Vys. Temp. 6, 921-922 (1968).
46. V. A. Gruzdev, R. E. Rovinskii, and I. P. Shirokova, "Some Properties of Stationary Electrodeless Discharge at High Pressures," Teplofiz. Vys. Temp. 5, 557-561 (1967).
47. V. A. Gruzdev, R. E. Rovinskii, and A. P. Sobolev, "An Approximate Solution for the Steady-State, Inductive-Type, High Frequency Discharge in a Closed Volume," Zh. Prikl. Mech. Tekh. Fiz. 1, 143-150 (1967).
48. H. J. Hedger and A. E. Hall, "Preliminary Observations on the Use of the Induction-Coupled Plasma Torch for the Preparation of Spherical Powder," Powder Met. 8, 65 (1961).
49. D. B. Henderson, "Aerodynamic Study of an Argon Plasma," Phys. Fluids 10, 1962-1967 (1967).
50. B. B. Henriksen, D. R. Keefer, and M. H. Clarkson, "Electromagnetic Field in Electrodeless Discharge," J. Appl. Phys. 42, 5460-5464 (1971).

51. W. Hittorf, "Ueber die Elektrizitäts-leitung der Gase," Ann. Physik 21, 90-139 (1884).
52. D. D. Hollister, "An Electrodeless Technique for Full-Scale Simulation of the Reentry Environment," Proc. 2nd Space Congr., April 5-7, 1965, Cocoa Beach, Florida, p. 549.
53. D. D. Hollister, "On the Electrodeless Arc in High-Pressure Air," Phys. Lett. 27A, 672-673 (1968).
54. D. D. Hollister, An Investigation of the High Pressure Electrodeless Arc in Air, Rept. AFFDL-TR68-160, AF Flight Dyn. Lab., Wright-Patterson AFB, Ohio (February 1969).
55. D. W. Hughes, A. Shamin, and E. R. Wooding, "Diffusion and Recombination in a Dense Argon Plasma," Paper presented Tenth Internatl. Conf. Phen. Ion. Gas., Oxford, England, 1971, Contrib. Papers, p. 243.
56. D. W. Hughes and E. R. Wooding, "The Temperature Distribution in an H-Mode RF Plasma Torch," Phys. Lett. 24A, 70-71 (1967).
57. P. D. Johnston, "Temperature and Electron Density Measurements in an RF Discharge in Argon," Phys. Lett. 20, 499-500 (1966).
58. P. D. Johnston, "Determination of Temperature in a Radio-Frequency Discharge Using a Reversal Technique," Brit. J. Appl. Phys. (J. Physics D) 1, 479-484 (1968).
59. D. R. Keefer, An Experimental Study of Electrodeless Arc Discharges, Report No. AEDC-TR-71-180, Arnold Engineering Division Center, Arnold Air Force Station, Tennessee (September 1971).
60. I. Kleinmann and J. Cajko, "Spectrophysical Properties of the Plasma of a High Frequency Discharge in Argon at Atmospheric Pressure," Spectrochim. Acta 25B, 657-668 (1970).
61. S. V. Kononov and M. I. Yakushin, "A Note Concerning the Determination of Specific Heat Fluxes Toward the Surface in the Air Jet of a High-Frequency Electrodeless Plasmatron," Zh. Prikl. Mekh. Tekh. Fiz. 6, 67-68 (1966).
62. E. F. Kustov and P. A. Arsen'ev "Initiation of High-Frequency Electrodeless Discharges," Zh. Tekh. Fiz. 37, 2167-2172 (1968).
63. S. L. Leonard, "Evidence for Departures from Equilibrium in an RF Induction Plasma in Atmospheric Pressure Argon," J. Quant. Spectrosc. Radiat. Trans. 12, 619-626 (1972).

64. F. Leprince-Ringuet, A. M. Lejus, and R. Collongues, "Sur la Preparation et la Fusion au Four a Plasma de Carbures, Nitrures et Oxynitrures Refractaires," C. R. Acad. Sci. Paris 258, Gr. 8, 221-223 (1964).
65. A. L. Levin and L. P. Poberezhskii, "Role of the Capacitance Between a Coil and a Plasma in Determining the Electrical Conductance of Plasma by Circuit Methods," Teplofiz. Vys. Temp. 5 769-777 (1967).
66. B. S. Malone and W. H. Corcoran, "Transition Probability Measurements in the Blue-Near UV Spectrum of Argon I," J. Quant. Spectrosc. Radiat. Trans. 6, 443-449 (1966).
67. P. J. Martenay, A. E. Mensing, and N. L. Crascella, Experimental Investigation of the Spectral Emission Characteristics of Argon-Tungsten and Argon-Uranium Induction Heated Plasmas, NASA Contr. Rept. CR-1314 (April 1969).
68. C. Marynowski and A. Monroe, RF Generation of Thermal Plasmas in High Temperature Technology, Butterworth and Co., Washington, (1964), 67-84.
69. B. E. Meierovich and L. P. Pitaevskii, "On the Structure of the Transition Layer in a High-Frequency Gas Discharge," Zh. Eksp. Teor. Fiz. 61, 235-242 (1971); also, Paper presented Tenth Internatl. Conf. Phen. Ion. Gas., Oxford, England, 1971, Contrib. Papers, 142.
70. A. E. Mensing and L. R. Boedeker, Theoretical Investigations of RF Induction Heated Plasmas, NASA Contr. Rept. CR-1312 (April 1969).
71. B. E. Meyerovich, "On the Theory of An Equilibrium High-Frequency Gas Discharge," Zh. Eksp. Teor. Fiz. 61, 1891-1905 (1971).
72. R. C. Miller and R. J. Ayen, "Temperature Profiles and Energy Balances for an Inductively Coupled Plasma Torch," J. Appl. Phys. 40, 5260-5273 (1969).
73. A. Mironer and F. Hushfar, "Radio-Frequency Heating of a Dense, Moving Plasma," Paper 63045-63 AIAA Electric Propulsion Conf., Colorado Springs, Colo., March 11-13, 1963.
74. R. V. Mitin and K. K. Pryadkin, "A High Pressure Electrodeless Discharge," Zh. Tekh. Fiz. 35, 1205-1209 (1965).
75. R. V. Mitin and K. K. Pryadkin, "Magnetic Properties of a High Pressure Electrodeless Discharge," Zh. Tekh. Fiz. 36, 913-919 (1965).

76. R. V. Mitin and K. K. Pryadkin, "Magnetic Field Influence on High Pressure Electrodeless Discharge Plasma," Proc. 8th Interntl. Conf. Phen. Ionized Gases 249, Vienna (1967).
77. R. V. Mitin and K. K. Pryadkin, "Effect of a Magnetic Field on the Plasma of Electrodeless Discharges," Teplofiz. Vys. Temp. 8, 1142-1148 (1970).
78. F. Molinet, "Etude de la Repartition de la Temperature Electronique a L'interieur d'un Plasma d'Argon Produit par un Generateur H. F.," C. R. Acad. Sci. Paris Ser. B 262, 1377-1380 (1966).
79. J. W. Poole and Ch. E. Vogel, Induction Plasma Nozzle Tests, NASA Contractor Rept. CR-1765 (April 1971).
80. D. C. Pridmore-Brown, "A Numerical Study of the Inductive Electrodeless Discharge," J. Appl. Phys. 41, 3621-3625 (1970).
81. K.K. Pryadkin, R. D. Mitin, and N. N. Klimov, "Electrodeless Discharge in Xenon at Pressures up to 40 atm." Zh. Prikl. Spektrosk. 10, 721-724 (1969).
82. R. G. Ragsdale and C. D. Lanzo, "Reentry Heating Experiments Using an Induction Heated Plasma," NASA TMX-1978, March 1970.
83. Yu. P. Raizer, "High-Frequency Discharge in a Gas Flow as a Process of Slow Burning," Zh. Prikl. Mekhan. Tekhn. Fiz. 3, 3-10 (1968).
84. Yu. P. Raizer, "High-Frequency, High Pressure Induction Discharge and the Electrodeless Plasmatron," Usp. Fiz. Nauk 99, 687-712 (1969).
85. T. B. Reed, "The Induction Coupled Plasma Torch," J. Appl. Phys. 32, 821-824 (1961).
86. T. B. Reed, "Growth of Crystals Using Induction Plasma Torch," J. Appl. Phys. 32, 2534-35 (1961).
87. T. B. Reed, "Heat-Transfer Intensity from Induction Plasma Flames and Oxy-Hydrogen Flames," J. Appl. Phys. 34, 2266-2269 (1963).
88. T. B. Reed, "Chemical Uses of Induction Plasmas," p. 26-34 in The Application of Plasmas to Chemical Processing, ed. R. F. Baddour and R. S. Timmins, The MIT Press, Cambridge, Mass. (1967).
89. W. C. Roman and J. F. Klein, "Investigation of High Pressure, Vortex Stabilized RF Plasma Discharges," Paper No. 69-695, AIAA Fluid and Plasma Dynamics Conf., San Francisco, California, June 16-18, 1969.

90. W. C. Roman, "Investigation of an RF Radiant Energy Source with Uranium Hexafluoride and Tungsten Injection," Paper presented 2nd Symp. Uranium Plasmas: Research and Applications, Atlanta, Ga., November 15-17, 1971, Collection of Papers, 239-246.
91. R. E. Rovinskii and A. P. Sobolev, "Optimum Frequency Range of a Stationary Induced Discharge," Teplofiz. Vys. Temp. 6, 216-219 (1968).
92. R. E. Rovinskii and A. P. Sobolev, "Calculation of the Parameters of an Induced High-Frequency, High Pressure Discharge," Teplofiz. Vys. Temp. 7, 203-207 (1969).
93. R. E. Rovinskii and A. P. Sobolev, "Application of the Channel Model and the Minimum Principle to an Induced Discharge," Teplofiz. Vys. Temp. 9, 30-36 (1970).
94. R. E. Rovinskii, L. E. Belousova, and V. A. Gruzdev, "The Geometry of Electrodeless Discharges Induced in Inert Gases," Teplofiz. Vys. Temp. 4, 328-335 (1966).
95. R. E. Rovinskii, V. A. Gruzdev, and I. P. Shirokova, "Energy Balance in a Stationary Induced Discharge," Teplofiz. Vys. Temp. 4, 35-39 (1966).
96. R. E. Rovinskii, et al., "Determination of Temperature in a Stationary High-Frequency Induction Discharge," Teplofiz. Vys. Temp. 5, 557-561 (1967).
97. P. D. Scholz and T. P. Anderson, "Local Thermodynamic Equilibrium in an RF Argon Plasma," J. Quant. Spectrosc. Radiat. Trans. 8, 1411-1418 (1968).
93. A. Shamin and E. R. Wooding, "Recombination in a Dense Argon Plasma," Phys. Letters 34A, 219-220 (1971).
99. C. G. Smith, "Studies of a Ring Discharge," Phys. Rev. 59, 997-1004 (1941).
100. V. N. Soshnikov and E. S. Trekhov, "On the Theory of the High-Frequency Turbulent Discharge at High Pressure II," Teplofiz. Vys. Temp. 4, 324-327 (1966).
101. V. N. Soshnikov and E. S. Trekhov, "The Theory of High-Frequency Vortex Discharges at High Pressure I," Teplofiz. Vys. Temp. 4, 166-172 (1966).

102. V. N. Soshnikov and E. S. Trekhov, "Contribution to the Theory of a High-Pressure Vortex Discharge in Air and Argon III," Teplofiz. Vys. Temp. 5, 522-525 (1967).
103. V. N. Soshnikov, et al., "Characteristics of a Long Induction Discharge in Argon at Atmospheric Pressure," Teplofiz. Vys. Temp. 9, 488-492 (1971).
104. A. Stokes, "The Ring Discharge Environment for Total Radiation Intensity and Thermal Conductivity Measurements," Proc. 8th Internatl. Conf. Phen. Ionized Gases, Vienna, 1967, 3.1.11.
105. A. D. Stokes, "Electrical Conduction and Radiant Heat Transfer in Induction Heating," Paper presented Internatl. Conf. on Gas Discharges, London, September 1970; IEEE Publ. No. 70, p. 182.
106. A. D. Stokes, "Thermal Equilibrium in Argon Induction Discharges," Brit. J. Phys. D.; Appl. Phys. 4, 916-925 (1971).
107. C. S. Stokes, et al., "Use of a Radio Frequency Plasma Jet in Chemical Synthesis," Am. Inst. Chem. Eng. J. 11 370 (1965).
108. J. J. Thomson, "The Electrodeless Discharge Through Gases," Philos. Mag. Ser. 7, Vol. 4, 1128-1160 (1927).
109. E. S. Trekhov, A. F. Fomenko, and Yu. M. Koshev, "Parameters of Stationary Inductive Discharges at Atmospheric Pressure," Teplofiz. Vys. Temp. 7, 860-865 (1969).
110. E. S. Trekhov, A. F. Fomenko, and Yu. M. Khoshev, "The Temperature Profile of the Plasma Column of an Induction Discharge in Argon at Atmospheric Pressure," Teplofiz. Vys. Temp. 8, 721-730 (1970).
111. N. Van Trong, "Recombinaison Electronique dans un Plasma d'Argon sous la Fression Atmospherique et an Voisinage de 10,000 K," C. R. Acad. Sci., Paris, Series B 264, 217-219 (1967).
112. C. Veillon and M. Margoshes, "An Evaluation of the Induction-Coupled, Radio-Frequency Plasma Torch for Atomic Emission and Atomic Absorption Spectroscopy," Spectrochim. Acta. 2, 503-512 (1968).
113. P. J. Vermeulen, W. L. Boddie, and F. A. Wierum, "State Control of a Flowing Plasma by Means of Radio Frequency Electromagnetic Field," AIAA J. 5, 1015-1917 (1967).
114. Ch. H. Vogel, "A Progress Report--Induction Plasma Simulation of the GCNR," Paper presented 2nd Symp. Uranium Plasmas: Research and Applications, Atlanta, Ga., November 15-17, 1971, Collection of Papers 170-172.

115. Ch. E. Vogel, Curved Permeable Wall Induction Torch Tests, NASA Contractor Rept. CR-1764, March 1971.
116. Ch. E. Vogel, J. W. Poole, and P. H. Dundas, Radiation Measurements and Low Frequency and High Pressure Investigations of Induction Heated Plasmas, NASA Contractor Rept. CR-1804 (May 1971).
117. F. B. Vurzel and L. S. Polak, "Plasma Chemical Technology - The Future of the Chemical Industry," Ind. Eng. Chem. 62, 8-22 (1970).
118. B. W. Walsh and A. D. Stokes, "Energy Balance and Stability of an Induction Heated Plasma," Chem. Eng. Sci. 27, 511-518 (1972).
119. R. H. Wendt and V. A. Fassel, "Induction Coupled Plasma Spectrometric Excitation Source," Anal. Chem. 37, 920-922 (1965).